Geophysical Journal International

Geophys. J. Int. (2016) **204,** 366–385 doi: 10.1093/gji/ggv433
GJI Marine geosciences and applied geophysics

Gravimetric determination of the continental–oceanic boundary of the Argentine continental margin (from 36°S to 50°S)

María Alejandra Arecco,[1] Francisco Ruiz,[2] Guillermo Pizarro,[2] Mario Giménez,[3] Patricia Martínez[3] and Víctor A. Ramos[4]

[1]*Instituto de Geodesia y Geofísica Aplicadas, Facultad de Ingeniería de la Universidad de Buenos Aires,* 2214 *Las Heras, Buenos Aires, Argentina. E-mail: arecco.ma@gmail.com*
[2]*Instituto Geofísico Sismológico Volponi, Facultad de Ciencias Exactas Físicas y Naturales, Universidad Nacional de San Juan, Ruta* 12 *Km* 17, *Jardín de los Poetas, Rivadavia, San Juan, Argentina*
[3]*Instituto Geofísico Sismológico Volponi, CONICET- Facultad de Ciencias Exactas Físicas y Naturales, Universidad Nacional de San Juan, Ruta* 12 *Km* 17, *Jardín de los Poetas, Rivadavia, San Juan, Argentina*
[4]*Instituto de Estudios Andinos (IDEAN), CONICET- Facultad de Ciencias Exactas y Naturales, Universidad de Buenos Aires,* 2160 *Intendente Güiraldes, Buenos Aires, Argentina*

Accepted 2015 October 5. Received 2015 October 4; in original form 2015 February 21

SUMMARY

This paper presents the gravimetric analysis together with seismic data as an integral application in order to identify the continental–oceanic crust boundary (COB) of the Argentine continental margin from 36°S to 50°S in a continuous way. The gravimetric and seismic data are made up of large grids of data obtained from satellite altimetry and marine research. The methodology consists of three distinct methods: (i) the application of enhancement techniques to gravimetric anomalies, (ii) the calculation of crustal thinning from 3-D gravity inversion modelling of the crust–mantle discontinuity and (iii) 2-D gravimetric modelling supported by multichannel reflection and refraction seismic profiles. In the first method, the analytic signal, Theta map, and tilt angle and its horizontal derivative were applied. In the second method, crustal thickness was obtained as the difference in the depths of the crystalline basement and the crust–mantle discontinuity; the latter was obtained via gravimetric inversion. Finally, 2-D modelling was performed from free-air anomalies in two representative sections by considering as restriction surfaces those coming from the interpretation of seismic data. The results of the joint application of enhancement techniques and 2-D and 3-D modelling have enabled continuous interpretation of the COB. In this study, the COB was determined continuously from the integration of 2-D profiles of the enhancement techniques, taking account of crustal thickness and performing 2-D gravimetric modelling. The modelling technique was complemented by regional studies integrated with multichannel seismic reflection and seismic refraction lines, resulting in consistent enhancement techniques.

Key words: Gravity anomalies and Earth structure; Composition of the continental crust; Composition of the oceanic crust; Continental margins: divergent; South America.

1 INTRODUCTION

The formation of the Argentine continental margin began in the Late Jurassic/Early Cretaceous (∼130 Ma) during the last stages of fragmentation of the supercontinent Gondwana, which took place from south to north, with the new South Atlantic Ocean opening between Argentina/Uruguay and South Africa/Namibia. This opening lasted from ∼137 Ma to 126 Ma (Rabinowitz & LaBrecque 1979; Menzies *et al.* 2002) and involved a complex combination of rifting and faulting before and during the South Atlantic breakup. This was accompanied by intense volcanic activity and the establishment of voluminous extrusive constructions and margin segmentation, and followed by seafloor spreading (Gladczenko *et al.* 1997; Hinz *et al.* 1999; Franke *et al.* 2007). A volcanic passive type margin (VPM) was thus generated between Rio Grande Rise and the Agulhas–Malvinas/Falkland fault, while at 50°S shear continental margin (SHM) type was generated, characterized by a prominent escarpment (Agulhas–Malvinas fault).

The VPM type is characterized by (i) having 60–120 km width, depending on the latitude or the segment, (ii) presenting seaward-dipping reflectors (SDRs; Hinz *et al.* 1999; Franke *et al.* 2010), (iii) having high-velocity lower-crust (HVLC) underplated bodies, which reach 7.8–8 km s^{-1} (Schnabel *et al.* 2008), (iv) presenting the development of rift and aulacogenic basins such as the Salado and

Colorado basins (Ramos 1996) and (v) presenting segments separated by Fracture Zones (Franke *et al.* 2007; Blaich *et al.* 2009). By contrast, the SHM is characterized by (i) presenting an extensive escarpment of 1100 km long and a maximum height of 2000 m high, corresponding to the Agulhas–Malvinas fault zone (Ramos 1996), separating two basements with different superficial characteristics, one high and straight and the other low and rough (Bird 2001), (ii) presenting a transition from oceanic (∼14 km thick) to continental crust (∼25 km thick) less than 50 km wide (Lorenzo & Wessel 1997) and (iii) having an evolution that typically involves continental rifting and deformed intensely rift sequences over rotated basement blocks (Bird 2001).

The main objective of this study is to determine the continental–oceanic boundary (COB) in a continuous way by means of a gravimetric–seismic analysis, applying enhancement techniques and inversion of the gravity field where there are isolated seismic data.

The knowledge of the nature and rifting process is of fundamental importance to understand the location of the continent–ocean boundary (COB). At volcanic margins, the ocean–continent transition occurs over short distances from 50 to 80 km (Mutter *et al.* 1982; White *et al.* 1987; White & McKenzie 1989) or from 120 to 150 km wide (Gladczenko *et al.* 1997; Dahl-Jensen *et al.* 1997). SDRs, large thicknesses of HVLC layers at volcanic margins have also been used to support mantle plume involvement and COB location (White & McKenzie 1989; Eldholm *et al.* 1995; Hinz *et al.* 1999; Schnabel *et al.* 2008; Tsikalas *et al.* 2012). On the continental shelf and the Argentine continental margin, seismic, gravity, and magnetic studies were performed to describe and characterize the sedimentary basins and the transition zones as those carried out by Ewing *et al.* (1963, 1964, 1971), Ludwig *et al.* (1968, 1978, 1979), Lonardi & Ewing (1971), Rabinovich & LaBrecque (1979) and Hinz *et al.* (1999). However, the COB has not been studied based on the analysis of crustal thickness. We incorporate seismic data containing information about the crustal and sediment thickness. The method of the implementing enhancement techniques and adding new seismic data, which are included in the 2-D modelling method, both methods improve the methodology of determining COB, because each method, through separate ways, obtain the same COB location.

It is expected to improve previous studies in the COB determination by making an analysis of the free-air anomalies field—gravimetric simplest expression—jointly with 2-D models and enhancement techniques. By analysing updated gravimetric grids from satellite altimetry, with the highest resolution and by combining seismic data, the regional COB determination by means interpolating the COB between transversal profiles to margin is improved.

2 GEOLOGICAL FRAMEWORK

The area studied comprises the Argentine continental margin between 35°S and 52°S and between 60°W and 45°W; that is, from the Rio de la Plata to the Malvinas Escarpment and from the shelf edge to beyond the continental slope (see Fig. 1A). The regional tectonic configuration of the margin comprises tectonic plates that constitute the oceanic expansion systems in South America, Africa and Antarctica. These components are the South American, African and Scotia plates, which are bounded by the Mid Atlantic, Rio Grande and North Scotia ridges.

The structure and tectonic evolution of the area studied have been described by Ramos (1996) and Urien & Zambrano (1996). This area has tectonic characteristics defined by its previous structural history, during which crustal discontinuities were originated over the period from the Transamazonian cycle (2300–1800 Ma) to the Gondwanic cycle (350–250 Ma), imprinting the VPM's own characteristics. This continental margin can be considered as a lower-plate passive margin (LPPM) type, with the upper-plate passive margin (UPPM) corresponding to the conjugate African margin. The main features characterizing the Argentine continental shelf as a lower-plate margin are its extensive shelves, the coastal plains in the continental terrace, well-developed half-graben systems, external peripheral ridge systems, a lack of well-developed basic magmatism and the presence of extensive rhyolitic plateaux (Ramos 1996).

The opening phase of the South Atlantic Ocean, with the oceanic crust formation, began in the Lower Cretaceous and it was diachronic, starting in the South (approximately 49°S) and gradually shifting North (Austin & Uchup 1982; Jackson *et al.* 2000; Franke *et al.* 2007). The estimated age for the opening between Argentina–Uruguay and South Africa–Namibia was approximately between the ranges 126 and 137 Ma (Gladczenko *et al.* 1997). West Gondwana broke up in Early Cretaceous times and subsequent seafloor spreading resulted in the formation of the South Atlantic Ocean. South America rotated clockwise with respect to Africa and it took almost 40 Ma, from earliest Valanginian to late Albian time, for Africa and South America to separate completely (Austin & Uchupi 1982; Franke 2013).

Continental breakup and initial seafloor spreading in the South Atlantic determined a volcanic passive margin (VPM) (36°S–48°S) and were accompanied by extensive transient magmatism as inferred from sill intrusions, flood basalt sequences, voluminous volcanic wedges (SDRs), and HVLC (Gladczenko *et al.* 1997; Hinz *et al.* 1999; Franke *et al.* 2007; Blaich *et al.* 2011; Franke 2013). Throughout Early Cretaceous (chron M10), the opening promoted the Agulhas–Malvinas/Falkland transcurrent fracture, one of the earth's most spectacular transform-Fracture Zone system (46.3°S, 10.0°W–46.9°S, 13.3°W) (Fig. 1); it also promoted that the 1200-km offset resulted in a giant class transform fault (Bird 2001).

Argentine continental margin can be divided into three frameworks according their tectonic settings, namely North, Middle, and South Frames (Lister *et al.* 1986; Ramos 1996). The northern and middle frameworks correspond to a lower plate passive margin, whereas the southern frame is characterised by the Malvinas Fracture Zone (Malvinas Escarpment) corresponding to the SHM.

According to Franke *et al.* (2007) the VPM can be divided into four segments (I, II, III and IV) bounded by the Malvinas/Falkland, Colorado, Ventana and Salado Fracture Zones (see Fig. 1A), which control the architecture, volume and width of the basaltic wedges which are SDRs (Hinz *et al.* 1999; Franke *et al.* 2007). These four interpreted Fracture Zones were confirmed on the basis of magnetic (Ghidella *et al.* 2002) and gravimetric data (Blaich *et al.* 2009). All segments belong to the North and Middle frameworks, according to Ramos (1996).

In segment IV, included in the North framework, parallel structures predominate towards Salado transfer zone, such as Martín García basement high, Punta del Este and Salado basins (Fig. 1A) and SDR's reach only 70 km wide. Segment III, included in the Middle Framework and bounded by the Salado and Ventana Fracture Zones, includes structures almost parallel to Salado and Ventana transference zones such as Claromecó and Colorado basins and Tandil basement high. The Ventana and Salado Fracture Zones control the SDRs which show around 80 km wide.

In the Middle Framework, segment II, the main feature is the submeridional development of the subparallel rift system to the shelf

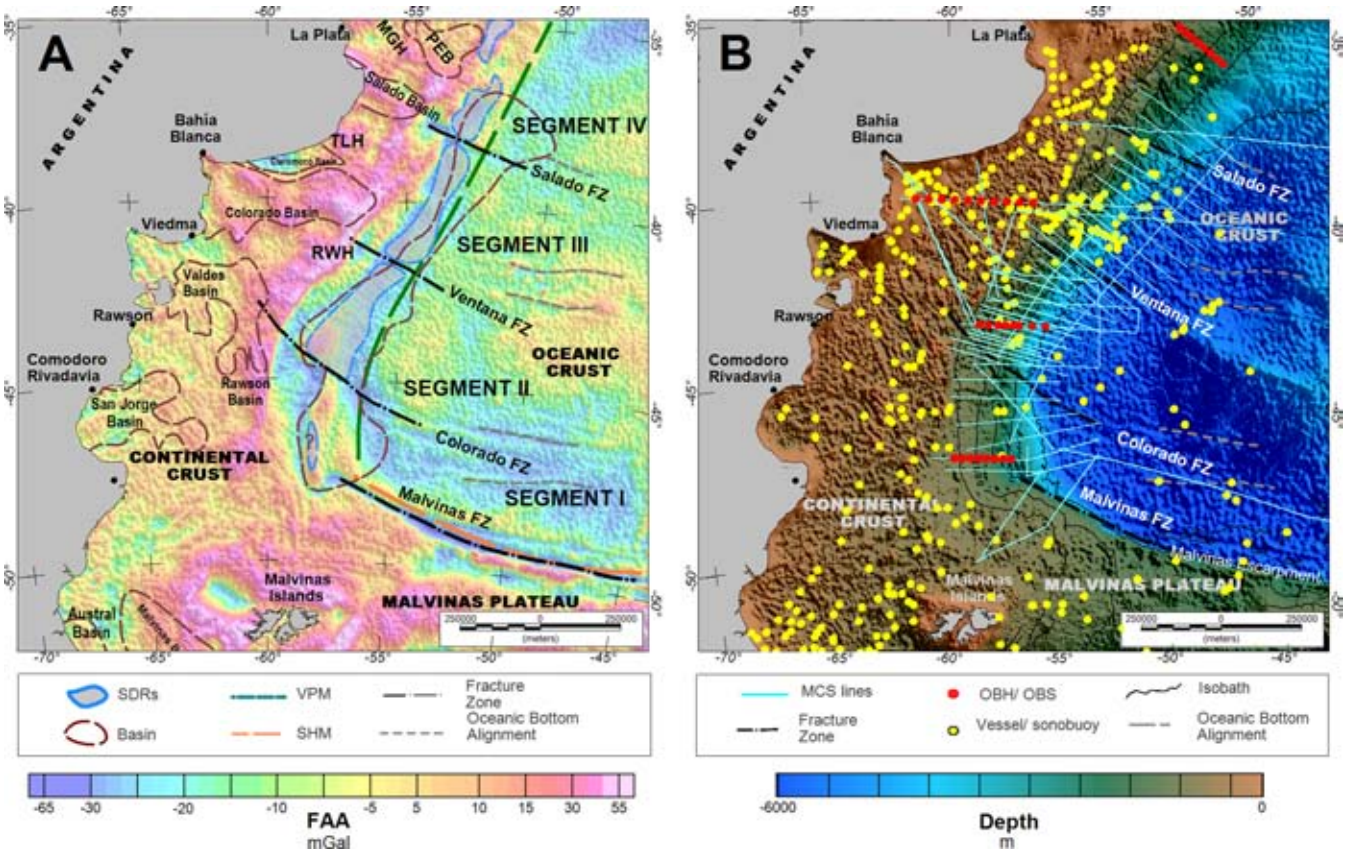

Figure 1. (A) Free-air anomalies from satellite altimetry (Sandwell *et al.* 2014). The volcanic passive margin (VPM) has a southwest–northeast orientation and the shear margin (SHM) has a west–east orientation. The main basins of the continental margin are based in Ramos (1996) and seaward-dipping reflector series (SDRs) according to Hinz *et al.* (1999) and Franke *et al.* (2007). (B) Bathymetric data from ETOPO1 grid (Amante & Eakins 2009) and reflexion/refraction seismic data. VPM, volcanic passive margin; SHM, shear margin; PEB, Punta del Este Basin; Salado FZ, Salado Fracture Zone; Colorado FZ, Colorado Fracture Zone; Malvinas FZ, Malvinas Fracture Zone; MGH, Martín García high zone; TLH, Tandil high zone; RWH, Rawson high zone; SDRs, seaward-dipping reflector series.

margin where it can be followed through the Península Valdés and Rawson basins (Ramos 1996). At northern to the Colorado Fracture Zones, this type of continental margin presents narrow margins and thick continental crust with an average continental thickness of 30 km, characterized by the intrusion of basaltic material at the bottom of the crust which is associated with a high-seismic velocity zone from 7.2 to 7.6 km s^{-1} below the basaltic horizon (e.g. HVLC) (Menzies *et al.* 2002; Schnabel *et al.* 2008). In this segment, the SDRs are the biggest, which reach 120 km wide (Hinz *et al.* 1999; Franke *et al.* 2007).

Whereas, segment I compared to previous segments, presents important changes in the morphostructural characteristics dominated by strike-slip movements, which probably prevent the generation of large volumes of melt (Franke *et al.* 2007). In this segment, SDRs are underdeveloped and have a sinistral displacement of about 100 km with respect to segment II across the Colorado TFZ (Franke *et al.* 2007; see Fig 1A).

The southern framework is characterized by presenting a prominent fault scarp corresponding to the Agulhas–Malvinas/Falkland fault zone and a deep ocean basin, located at the base of the transfer zone (Fig. 1B). According to Ramos (1996) and Ben-Avraham *et al.* (1993, 1997) the initial formation of this margin was active from the Middle to Late Jurassic Period and this offset endured for about 65 Ma (from 130 to 65 million years ago) until a major ridge jump reduced its size to about 180 km. The Malvinas/Falkland Plateau and Malvinas Basin are a complex of oceanic and continental blocks that travelled along the Algulhas-Malvinas/Falkland Fracture Zone after Middle Jurassic Gondwanide breakup of Antarctica from Africa and South America (Lorenzo & Wessel 1997; Bird 2001). Along the northern edge of the plateau, a prominent marginal ridge forms the Malvinas Escarpment and rises as much as 2 km over the South Atlantic Ocean (Fig. 1B).

Lorenzo & Wessel (1997) reported that the transition from oceanic (~14 km thick) to continental crust (~25 km thick) is less than 50 km wide in this continental shear margin. They have suggested that mechanical coupling and thermal subsidence of oceanic and continental crust, after the ridge segment passed, caused the continental side of the margin to bend down, while forcing the oceanic side to bend upward. Due to a series of ridge jumps, the offset has been reduced to about 290 km at the present day (Barker 1979; Tucholke *et al.* 1981). The present Malvinas/Falkland Transform is an intraoceanic feature located between 46.3°S, 10.0°W and 46.9°S, 13.3°W, that separates the South American and African sides of the Agulhas-Falkland/Malvinas Fracture Zone from each other (Fig. 1B). The transition zone from continental to oceanic crust is 52 km wide (profile distance 478 to 530 km), which is a typical value for sheared margins (Bird 2001). It is characterized by a sharp decrease in crustal thickness from 30 km on the continental side to 7 km on the oceanic side (Parsiegla *et al.* 2007).

3 DATA

This study of the Argentine continental margin has a large amount of information, that consists of a bathymetric, gravimetric, magnetic, multichannel seismic data grids of 23 000 km, acquired in the Federal Institute for Geosciences and Natural Resources (*Bundesanstalt für Geowissenschaften und Rohstoffe*, BGR, Germany) and 6900 km of multichannel seismic data from National Commission on the Outer Limit of the Continental Shelf (*Comisión Nacional del Límite Exterior de la Plataforma Continental*, COPLA, Argentina). These last new data grids were performed by extending the BGR profiles so that profiles of approximately 400 km in length were obtained. The bathymetric data consist of the depth and seabed topography, while the seismic data consist of seismic interpretation of: the depth and topography from crystalline basement, the full sedimentary thickness and its compressional wave velocities, SDRs and the HVLC bodies location and finally in some cross sections—depth and topography of the Moho. The gravimetric data consist of satellite altimetry (Sandwell *et al.* 2014) and profiles of the free-air anomalies from oceanographic surveys; the satellite altimetry data—continuous and uniform throughout the region—allowed carrying out regional studies; and profiles, allowed to performing 2-D detailed studies and to recognize the COB in enhancement techniques.

This study comprises bathymetric, gravimetric and seismic data. Bathymetric and gravimetric data were compiled from public sources. Most of the seismic data was also gathered from public sources and some was provided by COPLA. In particular, the velocities of compressional waves (Vp) in the Argentine Basin were provided by COPLA.

3.1 Bathymetric data

The seafloor depth in the studied area ranges from a few metres on the shelf up to values greater than 5000 m in the Argentine Basin. Part of bathymetric data were extracted from BGR and COPLA oceanographic surveys, and supplemented by marine surveys of the National Geophysical Data Center (NGDC) and the global digital grid ETOPO1 (Amante & Eakins 2009) gridded at a resolution of 1 × 1 arcmin size, available on the website of the National Oceanic and Atmospheric Administration (NOAA): http://www.ngdc.noaa.gov/mgg/global/global.html (Fig. 1B). The ETOPO1 grid provides seafloor topography derived from satellite altimetry combined with measurements of sea floor depth (Sandwell & Smith 2009). Although the accuracy of the seafloor topography has been the subject of discussion (Smith 1993; Smith & Sandwell 1994, 1997; Sandwell & Smith 2001, 2009), it is generally considered reliable at intermediate wavelengths (20 to 200 km) in areas where sediment coverage is thin (Sandwell & Smith 2001; Sandwell *et al.* 2014).

The shipboard survey lines sampled every 150 m (e.g. for mean latitude is 6 arc-sec), associated with gravity and bathymetry data are appropriate validate ETOPO1 and gravimetric data from satellite altimetry. In order to validate bathymetric model from satellite altimetry, the differences with more than 23 000 km of the BGR and COPLA surveys were calculated and analysed. The differences between ETOPO1 and model from surveys are close to 20 ± 4 m on the continental shelf and most differences ∼500 m are grouped around the continental shelf edge and in specific places (large slopes, little terraces or submarine canyons), therefore ETOPO1 model was used for completing the bathymetric final model and getting a uniform grid for 3-D regional studies; a sensitivity analysis to study how gravity anomalies are sensitive to bathymetry model can be seen in the Section 6. A map of the differences, between ETOPO1 and model from surveys, as additional material is presented (Annex A).

3.2 Gravimetric data

In this work, two main sources of free-air anomalies were used, a model from oceanographic surveys (from BGR and COPLA) and a newest global marine Gravity V23.1 model (Sandwell *et al.* 2014). The free-air marine gravity anomaly global grid is available in ftp://topex.ucsd.edu/pub/global_grav_1 min with a grid spacing of 30 × 30 arc-sec size and has an accuracy of about 2 mGal (Sandwell *et al.* 2014). The combination of new radar altimeter measurements from CryoSat-2 and Jason-1 with existing data has allowed constructing a global marine gravity model that is two times more accurate than previous models (Sandwell *et al.* 2014).

In order to validate free-air anomalies from satellite altimetry data, in the same way as in Section 3.1, the satellite altimetry data was compared with more than 23 000 km of geophysical surveys from BGR and COPLA. The differences of the global marine Gravity V23.1 model in relation to ships gravity data approximately reached ± 2 mGal in the continental shelf, ± 8 mGal in the continental slope and Malvinas Escarpment, ± 12 mGal in small and particular places as large slopes, little terraces or submarine canyons, and ± 2 mGal in abyssal plain, which were sufficient for validating the global model.

The gravity model resulted by means of geophysical surveys from BGR and COPLA data (Fig. 1A), and supplemented with global marine Gravity V23 model (Sandwell *et al.* 2014).

Moreover, sensitivity studies were performed, these consisted in calculating how gravity varies with an oscillation of ±20 m in the depth that represents ±1.1 mGal (at continental shelf), and in calculating a discrepancy in ±100 m that represents approximately ±6 mGal (at Argentine basin), wherewith it was considered that shipboard surveys lines have enough resolution for studying 2-D profiles. For 3-D bathymetric/gravimetric models the same studies were applied and the similar results were obtained, so that 3-D bathymetric/gravimetric models keep enough accuracy for the regional studies. A map of the differences, between global marine Gravity V23 model and the model from surveys, as additional material is presented (Annex B).

3.3 Seismic data

Seismic data were collected from several institutions: from the Lamont Doherty Earth Observatory (LDEO, United States) for the 1960s and 1970 s, whose results were partially published by Ewing *et al.* (1963, 1964, 1971), Leyden *et al.* (1971), Lonardi & Ewing (1971), Kowsmann *et al.* (1977); that institution in collaboration with Argentina's Naval Hydrographical Service (*Servicio de Hidrografía Naval* or SHN), whose data were published by Ludwig *et al.* (1968) and Ewing & Lonardi (1971) (Fig. 1B); from collections published by Urien & Zambrano (1970, 1996), Urien & Ewing (1973) and Ludwig *et al.* (1978); the most recent seismic data (from 1987 to 2004) from the Federal Institute of Geosciences and Natural Research (Hannover, Germany) during the surveys BGR-87, BGR-98 and BGR-04 whose results were partially published by Hinz *et al.* (1999), Franke *et al.* (2002, 2007, 2010), Schnabel *et al.* (2008), and Soto *et al.* (2011); and for the years 2001–2002 from COPLA (unpublished). The seismic data set came from multichannel seismic (MCS) reflection and seismic refraction from different sources

such as vessels, sonobuoys, ocean-bottom seismometers (OBS) and ocean-bottom hydrophones (OBH; Fig. 1B).

All this information provided data about the thickness of sedimentary basins on the large continental shelf, the depth and shape of SDRs, the depth of the crust–mantle discontinuity and the Argentine Basin thickness, located beyond the continental slope. The crystalline basement's depth was compiled from MCS lines (Fig. 1B) partially published by Hinz *et al.* (1999), Franke *et al.* (2002, 2007, 2010), Schnabel *et al.* (2008), and Soto *et al.* (2011). The collection of these data made possible to produce a grid of crystalline basement depth and sediment thickness of 1 × 1 arcmin resolution whose representation is shown through their isopachs every 1000 m (Fig. 1B).

The methodology for the capture, analysis and interpretation of seismic refraction used in stations or radio sonobuoys and conducted by the LDEO is described in the publications mentioned above. The registration and processing of seismic data obtained by BGR is described in Franke *et al.* (2007) and Neben & Schreckenberger (2005). BGR and COPLA surveys were converted to depth according to the law of Ludwig *et al.* (1978) and the crystalline basement was interpreted to determine the sediment thickness (unpublished).

The depth of the crust–mantle discontinuity was taken only at the positions where it was clearly interpreted (8 km s^{-1}) in seismic refraction information (Fig. 1B). The model of sediment densities derives primarily from the use of Gardner's empirical velocity-density relation (Brocher 2005) for sedimentary units and Christensen & Mooney (1995) for crystalline continental crust.

4 METHODS

Three different gravimetric methods were applied, which were independent of each other, in order to continuously outlining the COB zone: the application of enhancement techniques to gravimetric anomalies in 3-D, the determination of crustal thinning and finally gravimetric modelling in 2-D. The COB was then determined on 20 profiles by applying these techniques, and then extrapolated to span the entire continental margin.

The gravimetric field was extracted from the satellite altimetry free-air anomalies grid using a 30 × 30 arc-sec size cell (Sandwell *et al.* 2014), however this work focuses on the gravitational effects of deep crustal sources; therefore, the corrected Bouguer anomalies, that normalize the upper crust, were used because of their relationship with the upper mantle in the techniques described below.

4.1 Topographical and geological corrections of Bouguer anomalies

From free-air anomalies, Bouguer anomalies were calculated and corrected by the seafloor topography in order to extract the gravimetric effect of the water layer (Bouguer anomalies with topographical correction, BA_{TC}; see LaFehr 1991; Hinze *et al.* 2005); Bouguer anomalies corrected by seafloor topography were obtained from eq. (1):

$$BA_{TC} = FAA + C_T \tag{1}$$

where BA_{TC} are Bouguer anomalies corrected by seafloor topography, FAA are free-air anomalies, and C_T is the topographic correction.

Terrain correction was calculated using the module Oasis Montaj that uses the algorithm proposed by Nagy (1966) and Kane (1962). To calculate corrections, the ETOPO 1 was 'sampled' to a grid mesh centred on the station to be calculated. The correction was calculated based on near zone, intermediate zone and far zone contributions. In the near zone (0 to 1 cells from the station), the algorithm sums the effects of four sloping triangular sections, which describe a surface between the gravity station and the elevation at each diagonal corner. In the intermediate zone (1–8 cells), the terrain effect is calculated for each point using the flat topped square prism approach of Nagy (1966). In the far zone, (greater than 8 cells), the terrain effect is derived based on the annular ring segment approximation to a square prism as described by Kane (1962). However, terrain corrections for Shipborne/Airborne survey are calculated using the flat topped square prism approach of Nagy (1966) for all near zone, intermediate zone and far zone.

The topographic correction derived from the seafloor topography can be calculated by assuming that the water body is replaced by rock material and then subtracting the gravitational attraction caused by the water body. In order to evaluate the topographic effect caused by the seafloor topography (C_T) the algorithm from Nagy (1966) was used. Nagy (1966) developed a computer subroutine for a rectangular prism as a unit building block.

Topographic correction (C_T) was computed from free-air marine gravity anomaly global grid, the ETOPO1 grid of sea depths and the density of sea water, 1030 kg m^{-3} (Hinze *et al.* 2005), by direct modelling of the volume of water from sea level to the seafloor using a contrast density of 1640 kg m^{-3}, accounting for the effect of the earth's curvature (La Fehr 1991; Hinze *et al.* 2005).

Subsequently, Bouguer anomalies were calculated by subtracting the geological correction (BA_{GC}), which completes the normalization of the upper crust; that is, anomalous effects produced by sedimentary basins were eliminated from the gravimetric signal. The quantity BA_{GC} then contains the most significant effects, mainly the gravimetric effect of the crust–upper-mantle discontinuity. This calculation is performed using eq. (2) (Ruiz & Introcaso 1999; Hofmann-Wellenhof & Moritz 2006):

$$BA_{GC} = BA_{TC} - C_G, \tag{2}$$

where BA_{GC} are Bouguer anomalies corrected by sediment thickness, BA_{TC} are Bouguer anomalies corrected by seafloor topography and C_G is the geological or gravimetric effect of the sediment thickness.

Parker's algorithm (1972), implemented in the GM-SYS 3-D software, was used to calculate the gravitational effect of sediment thickness, C_G, by direct modelling. The sedimentary volume and density for the sediments volume was obtained from the database (see Section 3.3) and density was calculated from the velocities of compressional waves (v_i) from MCS surveys, specifically from the BGR (1998) and the COPLA (2001), and the ratio of Gardner *et al.* (1974). The obtained density was calculated as follows:

(1) From multichannel seismic profiles, columns of n thickness intervals were taken every 5 km, each interval having an associated compressional wave velocity; the weighted velocity $V_{weighted}$ of each column was then calculated according to eq. (3):

$$V_{weighted} = \frac{\sum_{i=1}^{n} th_i v_i}{\sum th_i}, \tag{3}$$

where $V_{weighted}$ is the weighted velocity of the sedimentary column, th_i is the thickness of the interval i, v_i is the compressional velocity of the interval i and n is the number of intervals in each column.

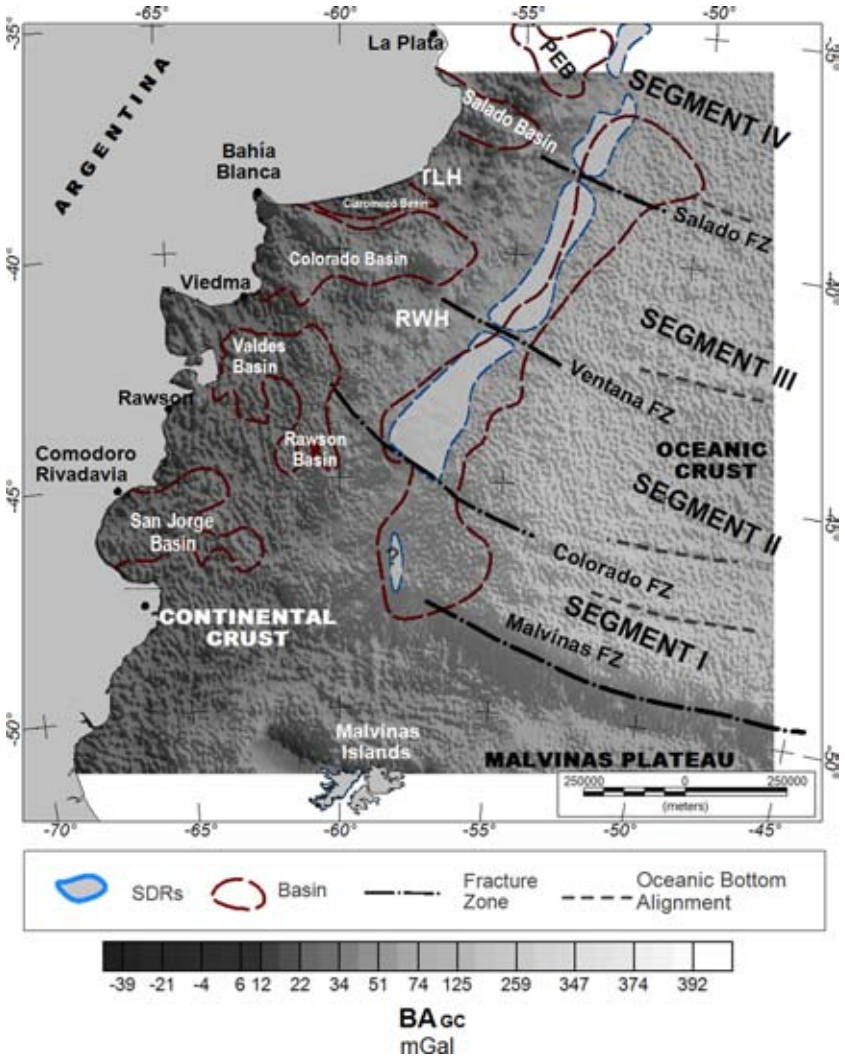

Figure 2. Bouguer anomalies with geological correction. The Bouguer anomalies were calculated and corrected by geological correction. BA_{GC} map shows positive values which realize make clear the crustal thinning, as well as, under both Colorado and Salado basins on the continental shelf, and on deep Argentina basin. For references see Fig. 1(A).

The calculation of V_{weighted} was repeated for each column in order to calculate the average velocity V_{average} of all the columns of all profiles according to eq. (4):

$$V_{\text{average}} = \frac{\sum_{j=1}^{m} V_{\text{weighted}\,j}}{m}, \tag{4}$$

where V_{average} is the average velocity of V_{weighted} and m is the number of columns in all profiles.

(2) Gardner's relation (Brocher 2005), which relates the compressional velocities with the sediments densities, was used to calculate the average density (ρ) of sediments in the Argentine Basin ($\rho = 2450\ \text{kg m}^{-3}$).

Finally by subtracting the BA_{TC} grid, from the CG grid, the Bouguer anomalies with geological correction (BA_{GC}) were obtained (Fig. 2).

4.2 Enhancement techniques

Enhancement techniques were applied to the gravimetric field in the continental margin in order to reveal the lateral density variations in deep structures between continental, oceanic and transition crusts, edges of the transitional crustal typical structures as the high velocity of the lower crust, SDRs, or feeding dykes zones, that are typical feature of volcanic rifted margins (e.g. Korenaga *et al.* 2001; Schnabel *et al.* 2008), were detected.

4.2.1 Analytic signal

This technique was developed in 2-D by Nabighian (1972, 1974) to be applied to the potential magnetic field as a procedure for resolving magnetic anomalies through Fourier transform. The Fourier transform in the frequency domain allows the determination of the vertical derivative of potential field from its horizontal derivative and the inverse Fourier transform is the function analytic signal (AS), whose real part is the horizontal derivative of the field profile and whose imaginary part is the vertical derivative of the field profile (Nabighian 1972). The real and imaginary parts of an analytic signal are real-valued functions related to each other by the Hilbert transform. Subsequently, the same author generalized the analytic signal from 2-D to 3-D (Nabighian 1984) through generalized Hilbert transform. Roest *et al.* (1992) applied 3-D analytic

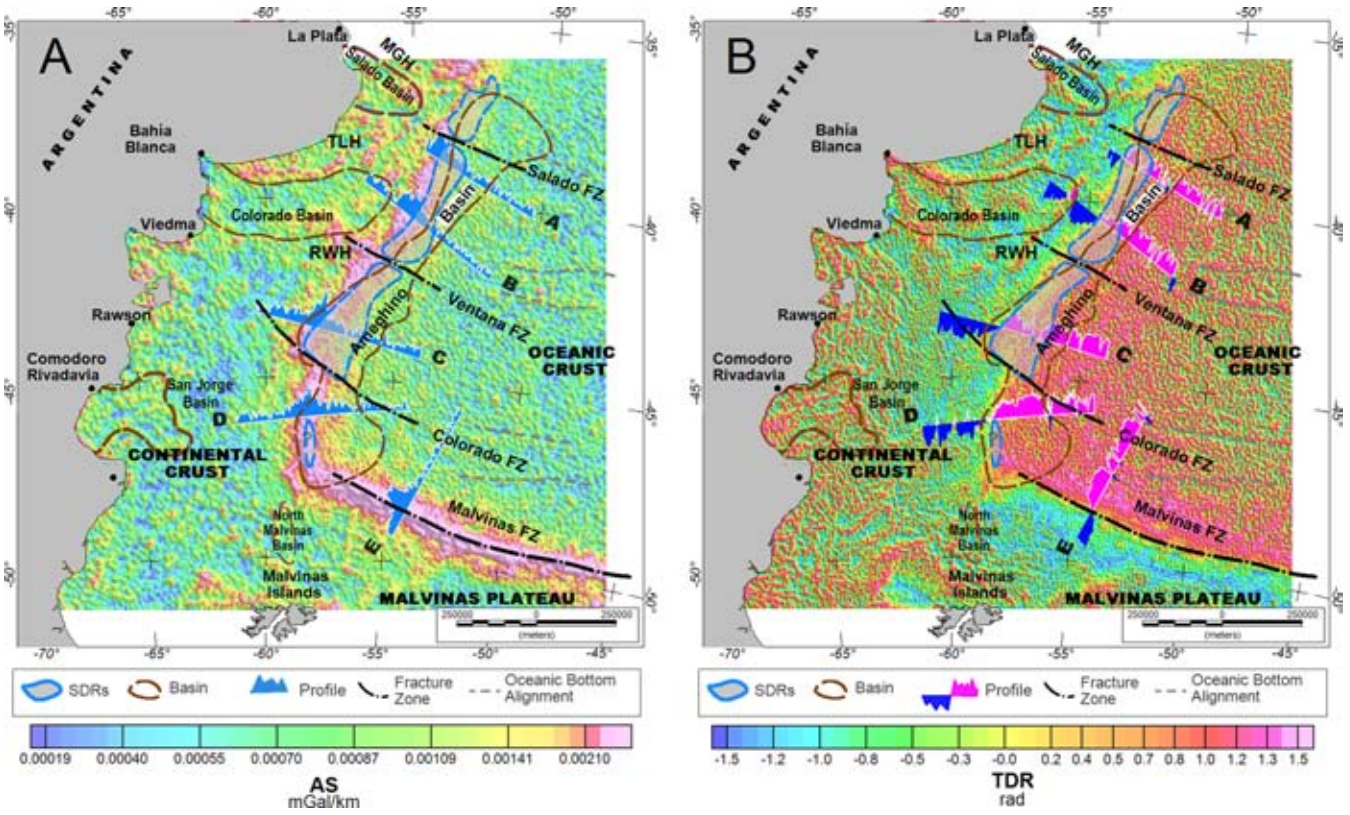

Figure 3. Enhancement techniques applied to the Argentine continental margin. (A) Analytic signal (AS) and (B) tilt angle (TDR) maps are shown. In both maps, five transverse rotated profiles of the respective applied techniques, major Fracture Zones and the most significant sedimentary basins according to their gravitational weight are shown. For references see Fig. 1(A).

signal as a magnetic interpretation method and Hansen *et al.* (1987) used the 3-D analytic signal in the interpretation of gravity data.

The advantage of using the absolute value of the analytical signal, is that its shape over linear structures is independent of the earth' s magnetic field parameters and the direction of magnetization of the source material (Roest *et al.* 1992). In particular, the modulus of the analytic signal in 3-D,$|\mathrm{AS}(x, y)|$ —also called the total gradient (Nabighian *et al.* 2005)—has been used like a normalizing factor in many filters, in the Theta map (Wijns *et al.* 2005) or in the local wavenumber (Thurston & Smith 1997). Its 3-D application has also been extended to the potential gravimetric field for the enhancement of potential field anomalies over kimberlite pipes and meteorite impact sites (Cooper 2009). The amplitude of the AS in 3-D is given by eq. (5):

$$|\mathrm{AS}(x, y)| = \sqrt{\left(\frac{\partial \mathrm{BA_{TC}}}{\partial x}\right)^2 + \left(\frac{\partial \mathrm{BA_{TC}}}{\partial y}\right)^2 + \left(\frac{\partial \mathrm{BA_{TC}}}{\partial z}\right)^2}, \qquad (5)$$

where $\frac{\partial \mathrm{BA_{TC}}}{\partial x}$ and $\frac{\partial \mathrm{BA_{TC}}}{\partial y}$ are the horizontal derivatives and $\frac{\partial \mathrm{BA_{TC}}}{\partial z}$ is the vertical derivative of the Bouguer anomalies with topographic correction ($\mathrm{BA_{TC}}$). The real parts of complex analytic signal are $\frac{\partial \mathrm{BA_{TC}}}{\partial x}$ and $\frac{\partial \mathrm{BA_{TC}}}{\partial y}$ and the imaginary part is $\frac{\partial \mathrm{BA_{TC}}}{\partial z}$. The results of applying eq. (5) include a wide area of maximum amplitudes associated with the continental slope and the type of continental margin (Fig. 3A).

The 3-D application of $|\mathrm{AS}(x, y)|$ is effective on the shelf because it is sensitive to such minor structures as the Colorado sedimentary basin boundary represented by narrow alignments of maximum warm colour (Fig. 3A), high areas in Martín García, Tandil and Rawson, and subparallel alignments associated with seafloor spreading (Fig. 3A).

Five rotated profiles (A, B, C, D and E) which are transverse to the VPM were plotted in order to show the amplitude and wavelength of $|\mathrm{AS}(x, y)|$ (Fig. 3A). These profiles exhibit great amplitude and wavelength (∼120 km); it assumed that these features are due to the density and distribution of internal sources that constitute the crustal edge as HVLC and deep magmatic intrusions (Fig. 3A). However, profile E, which is transverse to the shear margin or Malvinas Fracture Zone, exhibits large amplitude and shorter wavelength (∼50 km) due to the abrupt passage from continental to oceanic crust (Fig. 3A).

4.2.2 *Tilt angle*

The tilt angle, first introduced by Miller & Singh (1994), is defined by the relation of the potential field's first vertical derivative and the horizontal gradient, and is designed to uniformly enhance both subtle and prominent features (Nabighian *et al.* 2005). The tilt angle, denoted TDR by Verduzco *et al.* (2004), is defined in eq. (6), an equation similar to that giving the local phase of the analytic signal:

$$\mathrm{TDR} = \tan^{-1}\left(\frac{\mathrm{VDR}}{\mathrm{THDR}}\right), \qquad (6)$$

where TDR is the tilt angle and VDR and THDR are the first vertical derivative and horizontal gradient modulus respectively

of Bouguer anomalies with topographic correction according to eqs (7) and (8):

$$\mathrm{VDR} = \frac{\partial \mathrm{BA_{TC}}}{\partial z}, \tag{7}$$

$$\mathrm{THDR} = \sqrt{\left(\frac{\partial \mathrm{BA_{TC}}}{\partial x}\right)^2 + \left(\frac{\partial \mathrm{BA_{TC}}}{\partial y}\right)^2}, \tag{8}$$

where VDR can be positive or negative and THDR is always positive. In this paper, the tilt angle is applied as a method for locating the contact between the structures comprising the shelf and the continental boundary. The magnitude of the tilt angle passes through zero when it is directly over the edge of the source, at contact (Verduzco *et al.* 2004; Cooper & Cowan 2006).

As a result of the application of this technique, it was possible to highlight low-density sources located on the continental crust composed primarily of granite (negative or cold colours) compared to the ocean sources, mainly represented by basic rocks of greater density (positive or hot colour), so that they were isolated by the value zero (Fig. 3B).

Moreover, the tilt is sensitive to submeridian alignments related to the opening of the margin, marked on the map as Malvinas, Colorado or Salado Fracture Zones, and to some subparallel alignments associated with seafloor spreading (Fig. 3B).

Furthermore, this technique allows to emphasize low-density sources (sediments) on the continental crust (granitic composition), by recognizing gravimetric source boundaries related to the Salado, Colorado and Malvinas basins; while in the abyssal plain, volcanism is associated with seafloor spreading through the oceanic bottom alignments (Fig. 3B).

In the rotated profiles from A to D of Fig. 2B, tilt's zeros are expected to represent edges of deep sources like the continental crust narrowing; in the E profile is clearly seen that the zero tilt adjusts to the transcurrent margin area or Malvinas Fracture Zone.

However, due to the nature of the arctangent trigonometric function, all resulting angles are in the range between $-\pi/2$ and $\pi/2$ (Cooper & Cowan 2006), so details of other contacts whose angles has not been close to zero are lost. This technique effectively acts as a gain filter, since the trigonometric function induces clear discrimination around zero but loses definition away from this value.

4.2.3 Theta map

Although this technique is used to analyse the magnetic field, if one considers obliqueness of the field near the vertical, so that it eliminates distortion, an analogy occurs with the gravity field. The map of Theta (Wijns *et al.* 2005) is an edge detector given by eq. (9):

$$\cos(\mathrm{Theta}) = \frac{\mathrm{THDR}}{|\mathrm{AS}|}, \tag{9}$$

where the (positive) horizontal gradient amplitude,THDR, was defined in eq. (8) and the analytic signal amplitude, |AS|, was defined in eq. (5).

The Theta map can also be thought of as a normalization of the horizontal gradient. This filter enhances edges in data with any orientation instead of in those with a specific azimuth. A contact is defined in a profile as a maximum delimited by two minima. In the Theta map of the continental margin (Fig. 4A); maximum values are denoted by warm colours in a northeasterly direction, in contrast to contacts of the continental crust itself and the continental–oceanic transition (COT) in an east–west direction, the northern boundary of the Cretaceous Colorado Basin (Zambrano 1980) and the shear margin (Fig. 4A).

The Theta map can help determine the COB by discriminating contacts, with better definition than that provided by the tilt. The edges are detected, even with dipping, while the amplitude of the analytic signal does not capture these characteristics (Wijns *et al.* 2005). Franke *et al.* (2007) describe three series of SDRs with the western wedges being thicker. The location of the contacts of the main wedges is shown on the Theta map by alignment of maxima with warm colours parallel to the location of said wedges (Fig. 4A).

4.2.4 Total horizontal derivate of tilt (TDR_THDR)

As stated in Section 4.2.2, tilt results that are not adjacent to zero will have little or no representation. For this reason, the total horizontal derivative of tilt (TDR_THDR) was applied in order to improve the interpretation and to give a more accurate edge location for the oceanic crust. Verduzco *et al.* (2004) suggest using the horizontal derivative of tilt angle as an edge or contact detector in order to improve the results obtained by tilt (Fig. 4B). This total horizontal gradient of tilt is defined by (10):

$$|\mathrm{TDR\_THDR}| = \sqrt{\left(\frac{\partial \mathrm{TDR}}{\partial x}\right)^2 + \left(\frac{\partial \mathrm{TDR}}{\partial y}\right)^2}, \tag{10}$$

where TDR is the tilt angle of Bouguer anomalies with topographic correction ($\mathrm{BA_{TC}}$). This technique is independent of the source's direction, it enhances the anomalies, and the square root ensures the result is always positive. It works as an automatic gain control (Verduzco *et al.* 2004) which tends to increase the frequency in relation to tilt since it works as a high-pass filter enhancing subtle details with respect to the major details in the potential field data. This property is optimal for determining the beginning of the oceanic crust, characterized by a high degree of volcanism associated with seafloor spreading (Fig. 4B).

4.3 Crustal thickness

Crustal thickness is defined as the enclosed thickness between the surfaces of the crystalline basement (top) and the crust–mantle discontinuity (bottom). The crustal thinning was calculated by subtracting the Moho depth grid from the crystalline basement depth grid. The crystalline basement depth grid has been obtained from seismic data (see Section 3.3), whereas Moho depth grid has been calculated from gravimetric inversion (see Section 4.3.1). To calculate Moho grid depth, the gravimetric effect of the water and sediments layers from the free-air anomalies were isolated in order to get the effect of the crust and the mantle, that is, topographical and geological corrections of Bouguer anomalies were calculated.

Previous studies in the Colorado Basin utilized seismic recordings of the continental crust by BGR with ocean-bottom hydrophones, obtaining a result of ∼30 km thickness (Franke *et al.* 2006); in earlier gravimetric surveys in the basin, a thickness of ∼28 km was registered (Introcaso *et al.* 2003). Moreover, studies performed in across at section the continental shelf at 44°S and in the continental–oceanic crust transition showed that crustal thickness varies from ∼25 km to 14 km from west to east (Schnabel *et al.* 2008). In addition, the global average crustal thickness of igneous oceanic crust away from anomalous regions such as Fracture Zones

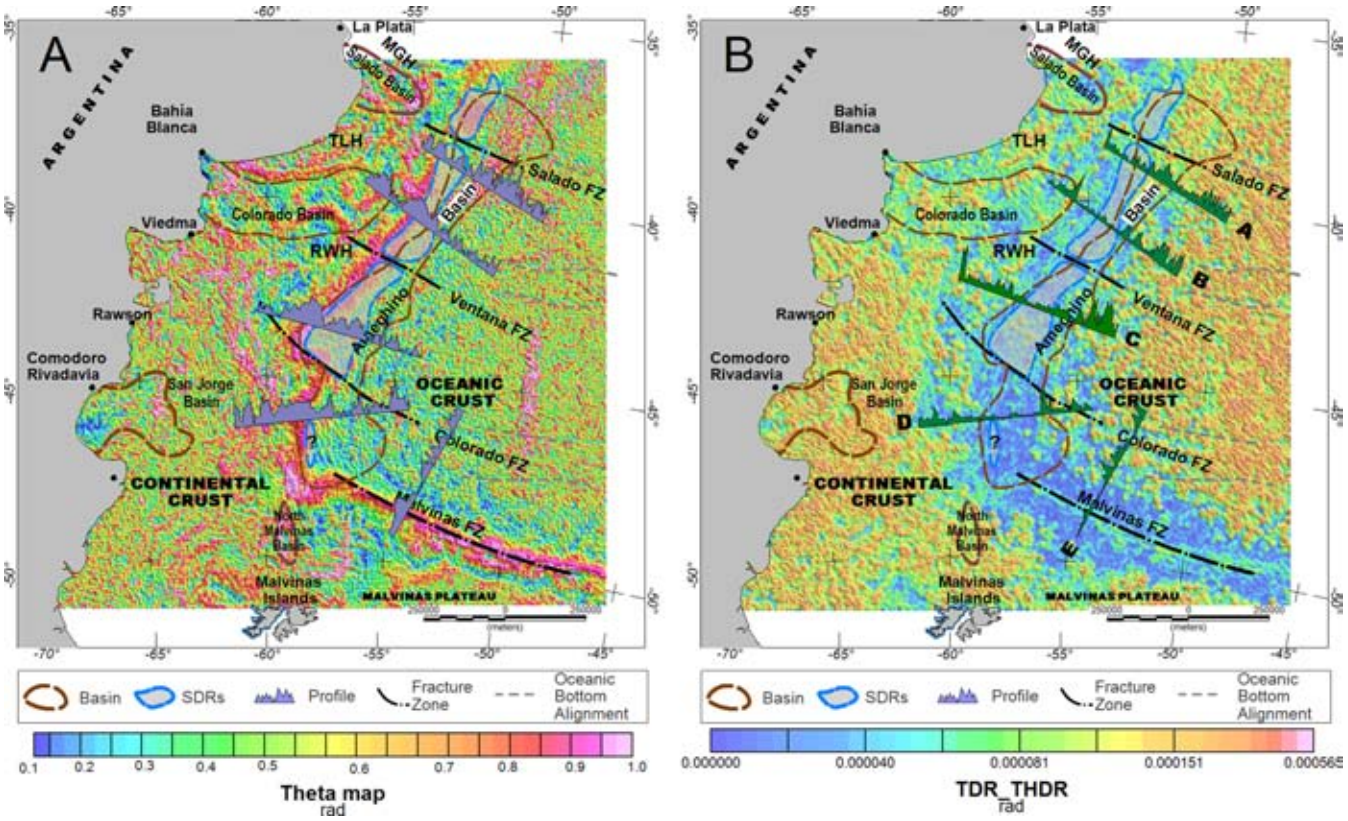

Figure 4. Enhancement techniques applied to the Argentine continental margin. (A) The Theta map amplitude enhances the edges of the major basins, the edge of the shelf and the Malvinas Escarpment. (B) The TDR_THDR map shows that the transition between the continental–oceanic crust and the transcurrent margin is narrower and better defined than the transition in the VPM. In both maps, the main sedimentary basins are shown, as are the area occupied by SDRs and alignments in the ocean seafloor. For references see Fig. 1(A).

and hot spots is $\sim 7 \pm 0.8$ km, with extreme limits of 5.0 to 8.5 km, according to White *et al.* (1992); north of the area, seismic refraction studies show thicknesses of 5 to 6 km (Leyden *et al.* 1971). Based on the above considerations, the edge of the transition crust by determining the 6 km isopach line is determined.

4.3.1 Crust–mantle discontinuity depth

Seismic data for the crust–mantle discontinuity depth is scattered and scarce due to seismic surveys offshore which purpose of exploring natural resources, generally study shallow sedimentary structures. In order to obtain the surface of the crust–mantle discontinuity in a continuous way for the entire region under study a 3-D Moho's depths model was calculated. This was considered an inversion problem of long-wavelength gravity anomalies.

Inverse problem and separation of the gravitational field, in order to obtain compensation depth, has been solved by Sampietro & Sansò (2012) considering that the topography and the crust density distribution are given and the depth of compensation is unknown. The bathymetry (seabed topography) and sediment were taken from external sources (not gravimetric sources), the densities of crust and mantle were considered as perfectly known and only the Moho's depth was inverted. In this case, theory says that the solution of the inverse problem is unique (see the second case by Sampietro & Sansò 2012). Data as geometric restrictions or constrains such as seismic information and density contrast, according to Hinze *et al.* (2005), and geophysics and geologic data was imposed; finally the results were compared and validated with the deep seismic data presented earlier. A new model of Moho depth based on inverting gravimetric data was introduced – called Argentine Marine Moho by Gravimetric Inversion (AMGI) – (see Fig. 4A).

The crust–mantle discontinuity depth was obtained by gravimetric inversion from filtering and inverting iteratively. Filtering consisted of calculating the upward continuation that has operated as a low pass filter (Pacino & Introcaso 1987; Pacino 1989; Pawlowski 1995; Guo *et al.* 2013) of Bouguer anomalies with geological correction in the Fourier domain using Dirichlet's equation according to Dean (1958). Thus, Bouguer anomalies with geological correction represent the gravitational effect of the lower crust (Ruiz & Introcaso 1999; Lince Klinger *et al.* 2010).

Regional gravimetric field inversion from 25 km altitude, providing the surface depth of the crust–mantle discontinuity through a 3-D model in two layers: one representing the bottom crust (2900 kg m^{-3}) and the other representing the upper mantle (3300 kg m^{-3}; values taken from Introcaso *et al.* 2003).

Gravimetric inversion calculations were performed using the soft GMSYS 3-D based on the Parker algorithm (1972). The adjustment between the filtered field and the effect of the model was performed with the enhanced method of Caratori Tontini *et al.* (2008), which is based on a mathematical modification of the method (Parker & Huestis 1974; finally the result—called AMGI—can be seen in Fig. 5A.

The depth obtained with the crust–mantle discontinuity model showed a continuous uniform distribution grid with a resolution of 5 × 5 arcmin of cell-size (Fig. 5A), allowing calculation of the crustal thickness by contrast and difference with the

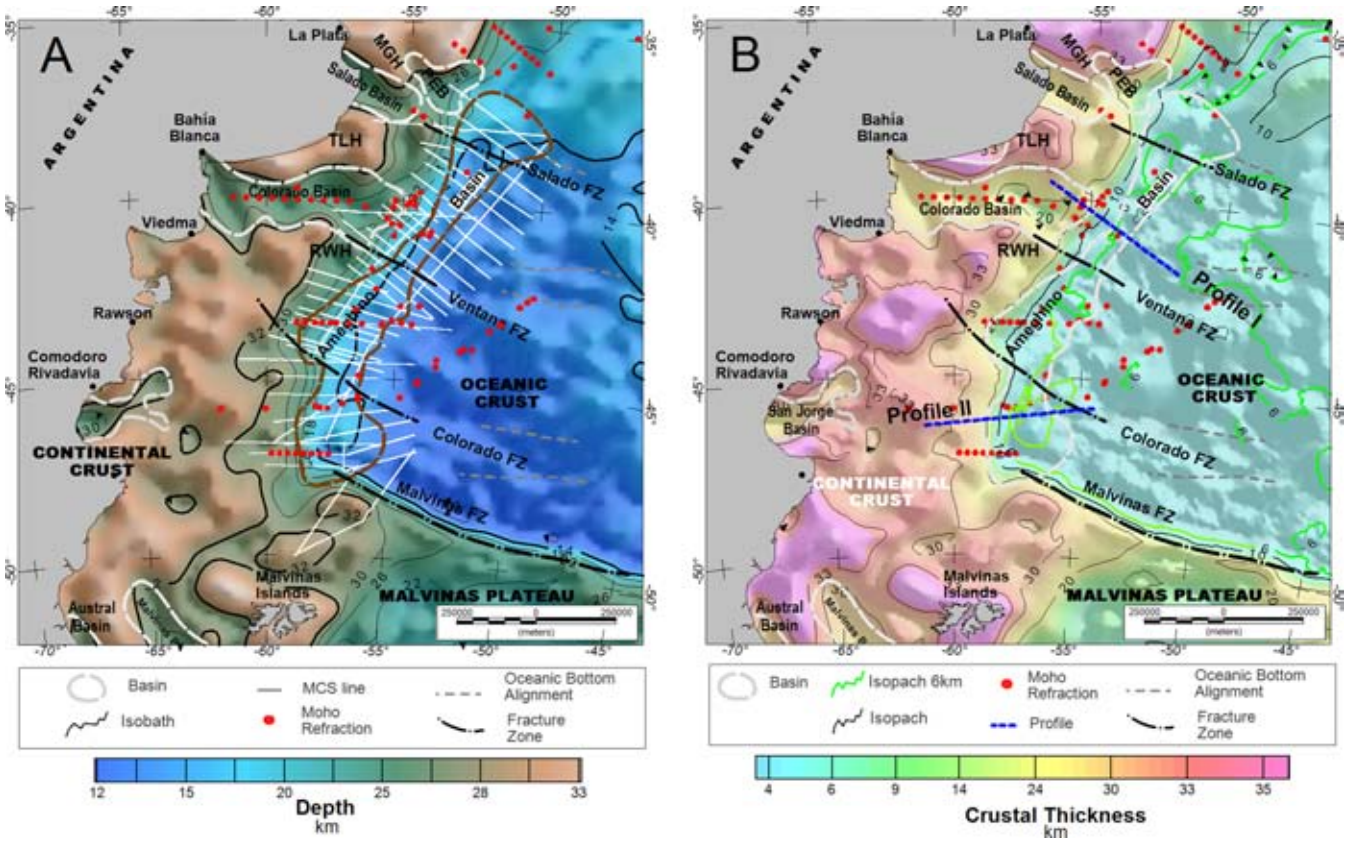

Figure 5. Map of (A) crust–mantle discontinuity depth and seismic refraction data locations; (B) crustal thickness and multichannel seismic locations. (A) Depth map shows Moho depths bellow continental crust 32 km, while below the oceanic crust ∼14 km (contours every 4 km). (B) Crustal Thickness map reveals the aulacogenic nature of the Salado and Colorado basins. The thicknesses under the San Jorge and Austral basins are reduced to a few kilometres; the isopach at 6 km (in green) characterizes the oceanic crust. Both maps also show the location of multichannel and seismic refraction data, Fracture Zones and ocean floor alignments. For references see Fig. 1(A).

basement from seismic data throughout the study area; results were compared and validated with deep seismic data presented earlier (Table 1).

According to Tarantola & Valette (1982), who examined the general non-linear inverse problem with a finite number of parameters using probability density functions for data parameters, it's note that the fact of having good geophysical data and geological assumption is in general not sufficient to guarantee the uniqueness. Ambiguity in gravity interpretation is inevitable because of the fundamental incompleteness of real observations; it is, however, possible to

Table 1. Comparison of the differences found between the depths of the crust–mantle discontinuity by reflection and refraction versus gravimetric inversion model (AMGI, Marine Argentine Moho by Gravimetric Inversion).

Publication	Max (km)	Min (km)	Mean (km)	RMS (km)
Seismic refraction				
AMGI–Moho in Ewing *et al.* (1963)	2.1	− 5.5	− 2.1	2.9
AMGI–Moho in Ewing *et al.* (1964)	1.2	− 2.4	− 0.8	0.9
AMGI–Moho in Ludwig *et al.* (1968)	0.1	− 0.7	− 3.2	2.8
AMGI–Moho in Ewing *et al.* (1971)	0.7	− 7.3	− 3.4	2.4
AMGI–Moho in Leyden *et al.* (1971)	− 1.1	− 4.2	− 3.1	1.7
AMGI–Moho in Ludwig *et al.* (1979)	3.0	− 4.4	− 0.1	2.0
AMGI–Moho in Franke *et al.* (2006)	7.7	0.6	4.7	2.2
AMGI–Moho in Schnabel *et al.* (2008)	3.2	− 1.3	1.0	1.7
Seismic reflection				
AMGI–Moho in Hinz *et al.* (1999)	2.2	− 1.3	0.1	1.0
AMGI–Moho in Franke *et al.* (2007)	6.1	− 4.4	1.3	1.2
AMGI–Moho in Franke *et al.* (2010)	5.2	− 1.2	2.0	2.3
AMGI–Moho in COPLA 2000–2001 (unpublished)	6.5	− 5.5	− 0.8	0.9

Table 2. Moho deep differences between AMGI and other models.

Differences between AMGI and other models	Max (km)	Min (km)	Mean (km)	RMS (km)
Gravimetric models				
AMGI–DMM (van der Meijde *et al.* 2015) South American model	9.4	−20.7	−0.6	3.7
AMGI–GEMMA (Reguzzoni & Sampietro 2015) Global model	15.1	−11.5	−4.1	2.8
AMGI–VMM (Bagherbandi *et al.* 2013) Global model	6.4	−20.5	−4.6	2.4
AMGI–GMSA12 (van der Meijde *et al.* 2013) South American model	6.4	−20.5	−4.5	2.4
Seismological models				
AMGI–CRUST1.0 (Laske *et al.* 2013) Global model	10.7	−23.5	−3.0	4.5
AMGI–Seismic structure of South America (Chulick *et al.* 2013)	8.3	−17.2	−1.4	3.4

provide rigorous limits on possible solutions even with incomplete data (Parker 1975).

This thickness clearly discriminates the continental crust (35–30 km) from the oceanic crust (10–13 km), by showing a significant gradient in the transition region (from ∼30 to ∼13 km). The model suggests crustal thickening north of the Salado transfer. The sinistral mass displacement is distinguished due to the Salado and Colorado transcurrent Fracture Zones. The model exhibits crustal attenuation related to the sedimentary Salado, Colorado and San Jorge basins. In the middle part of the Salado and Colorado basins, the crustal attenuation reaches 6 km and is joined by a stretch of 300 km parallel to the continental margin. The model is sensitive to the Malvinas Fracture Zones and the Colorado, Ventana and Salado basins.

On the other hand, a clear differentiation of the Malvinas Plateau is distinguished as compared to the continent, with decreased crustal thickness eastward of the Malvinas Islands, and an increased gradient steeper than in the VPM is seen on the shear margin along a length of 1000 km.

In the Gulf of San Jorge Basin, continuity to the continent related to the east–west alignment of the Malvinas Fracture Zone appears as a break in the crust–mantle discontinuity; this may be related to a crustal attenuation under the basin. Another explanation could be an increase in the density of the deep crust related to the area of Palaeozoic paleosubduction interpreted in the continent by Pankhurst *et al.* (2006) and Ramos (2008).

With the recently available high resolution gravity data from the GOCE satellite a whole range of crustal thickness models have been derived, such as DMM (van der Meijde *et al.* 2015), VMM (Bagherbandi *et al.* 2013), GEMMA (Reguzzoni *et al.* 2013) and GMSA12 (van der Meijde *et al.* 2013). Furthermore there are recent seismological models, such as CRUST1.0 (Laske *et al.* 2013) or Seismic structure of South America (Chulick *et al.* 2013). The different models of Moho depths for South America were compared to assess the quality of different modelling techniques and the impact of different data sources (see Table 2). The results of the evaluation are explained in the Section 6.

4.3.2 Crustal thickness computation

Crustal thickness model was calculated by subtracting the grid of the crust–mantle discontinuity depth (AMGI) from the grid of the interpreted crystalline basement surface depth (from Section 3.3) according to eq. (11).

$$\text{Crustal thickness} = \text{Basement depth} - \text{Discontinuity Moho depth}. \quad (11)$$

Eq. (11) (see Fig. 4B) allowed differentiation of a continental crust (∼30 km), a transition crust (30 km to 6 km) and an oceanic crust (∼6 km); the calculated thickness shows different narrowing gradients. In the case of the VPM there is a gradual or gentle slope and variable width (∼140–260 km) according to latitude; in the case of the shear margin the slope is steeper and its width is much smaller (∼10–25 km).

4.4 2-D gravimetric models

To overcome the non-uniqueness problem, it is possible to invert gravimetric data with a priori constrained information of the crustal structure (Nabighian *et al.* 2005), like discontinuities taken from seismic refraction method or interpreted seismic horizons from multichannel seismic profiles. In 2-D gravimetric models, for this inversion, it was assumed that simple crustal blocks are based on seismic data previously given in Section 3.3 and, on depth Moho by inversion given in Section 4.3.1, and also geological information consider the biggest structures in the continental margin such as low continental crust, upper continental crust among others. These constraints consisted in seafloor depths, collection of reflective surface depths interpreted in the seismic data as different sedimentary strata, crystalline basement, SDRs and HVLC, added to the crust–mantle discontinuity restrictions obtained in Section 3.3, which adjusted to the deep seismic data with satisfactory precision.

Although the same type of continental margin exists in both cases, there are significant differences in the edge effect gravimetric of anomalies north and south of the Colorado Fracture Zone; gravimetric models were conducted in two profiles, Profile I and Profile II, located north (38°S) and south (47°S) of the Colorado Fracture Zone, respectively; the locations of both are shown in Fig. 5B.

The basic architecture of the Profile I model (Fig. 6A) was taken from the Schnabel *et al.* (2008) and Arecco *et al.* (2014) model, which is 500 km to south of the Profile I; the architecture of the Profile II model (Fig. 6B) was modified from Neben & Schreckenberger (2005).

2-D modelling was used to overcome these differences, to establish the structures that characterize the margin, and specifically to identify the edge of the continental crust by exploiting enhancement methods for anomalies and extrapolating these characteristics to the entire region.

The gravimetric modelling needed to assign densities to blocks representing the most relevant structures Gravimetric modelling is mainly based on the assignment of a density and geometry to different blocks that represents the main crustal structures. These densities were extracted from reference works such as Introcaso *et al.* (2003) for seawater, upper and lower continental crust and the mantle as 1027, 2670, 2920 and 3300 kg m^{-3}, respectively. For sediment thickness, velocities of compressional waves converted to densities and Gardner's relation according to Brocher (2005) were used; and for igneous bodies, densities previous to Schnabel *et al.* (2008) were slightly modified.

In the modelling process, the interactive GravModeler program was used, which allows setting the observed gravitational anomaly

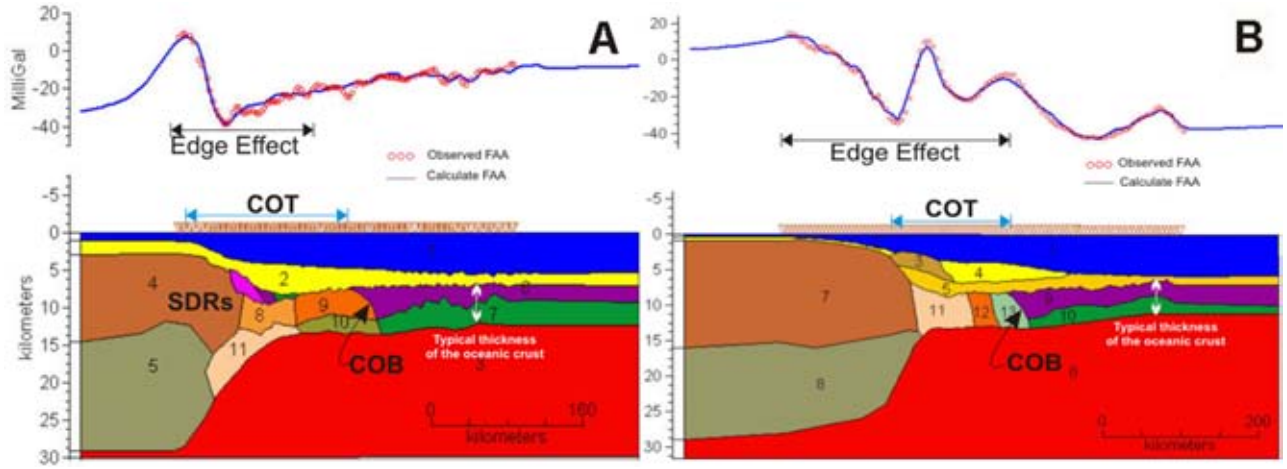

Figure 6. Gravimetric 2-D models in the VPM. (A) Profile I, Northern Colorado Fracture Zone; (B) Profile II, Southern Colorado Fracture Zone. The models represent a vertical section of the deep crust. Both profiles show observed gravity, calculated at less than 2.5 mGal (above), and bodies generating the calculated gravity (below). The edge effect in Profile II is influenced by the distribution of the sediment layers. The location of the profiles is shown in Fig. 5(B). The designations of blocks or bodies and respective densities are detailed in Tables 3 and 4. COT, continental–oceanic transition; COB, continental–oceanic boundary; SDRs, Seaward-dipping reflectors.

Table 3. Parameters used in Profile I (Fig. 6A).

No.	Unit	Density (kg m^{-3})
1	Seawater	1027
2	Sediment	2400
3	Mantle	3300
4	Upper continental crust	2670
5	Lower continental crust	2920
6	Upper oceanic crust	2870
7	Lower oceanic crust	2930
	SDRs	2740, 2750, 2780
8	Feeding dykes zone	2800
9	Upper transitional continental crust	2810
10	Lower transitional continental crust	2870
11	High-velocity lower crust (HVLC)	3150

Table 4. Parameters used in Profile II (Fig. 6B).

No.	Unit	Density (kg m^{-3})
1	Seawater	1027
2	Sediment I	2240
3	Sediment II	2410
4	Sediment III	2400
5	Sediment IV	2450
6	Mantle	3300
7	Upper continental crust	2670
8	Lower continental crust	2900
9	Upper oceanic crust	2800
10	Lower oceanic crust	2900
11	Transitional continental crust I	2790
12	Transitional continental crust II	2850
13	Transitional continental crust III	2890

to the calculated one by changing the geometry of the tectonic structures and by varying densities of the source blocks; the algorithm used to calculate the response on GravModeler is based on Talwani *et al.* (1959) algorithm implemented by Geotools Corporation (http://gravmodeler.software.informer.com/).

In this work the beginning/end of the profile were considered as its western/eastern side respectively. The COB in the Profile I model, defined as the contact between the transition crust and the oceanic crust, was found approximately 210 km from the beginning of the profile, where the lateral variation of density is 10 kg m^{-3} (Upper transitional continental crust – Upper oceanic crust), while the boundary in the Profile II model was found 300 km from the beginning of the profile, where the lateral variation of density is 20 kg m^{-3} (Transitional continental crust III – Upper oceanic crust).

Finally, the separation of the top and bottom crusts or other structures such as transition crusts and feeding dikes zones appeared in the model. The adjusted final densities of each of the bodies for each model are listed in Tables 3 and 4. The final architecture of both models is shown in Fig. 6.

The adjustment between observed and calculated gravity, the combination of architecture and modelled densities, were very satisfactory in Profile I and Profile II, since accuracy (in terms of Root Mean Square values) shows values lower than 1.9 and 2.5 mGal, respectively.

Again here the uniqueness is not guarantee by the algorithm, but can probably be claim that the solution is close to reality due to the large amount of data. Note also that the gravitational field is not perfectly fitted, probably a regularized least square solution for density of the different crustal bodies will allow improving the fitting (according to Tarantola & Valette 1982; Rossi 2013; Reguzzoni & Sampietro 2015; Rossi *et al.* 2015).

5 RESULTS

FAA map allow us to see the interrelation of the most conspicuous anomalies with the most relevant structures of the Argentine continental shelf (Fig. 1A), such as the Malvinas Plateau, continental basins (Punta del Este, Salado, Colorado, Malvinas and North Malvinas), deep basin margin (Ameghino Basin) and Fracture Zones (Salado, Colorado and Malvinas), as well as some basement highs (Martín García, Tandil and Rawson). Significant positive anomalies over the Colorado and Salado basins allow their interpretation as aulacogenic basins. This high positive gravimetric anomaly was attributed by Introcaso & Ramos (1984) and Introcaso (1990, 2003) to a dominant isostatic over compensation (i.e. to an excessively thinned continental crust beneath the basin).

In analytic signal map a slight change of direction occurs when passing through the Salado and Colorado Fracture Zones in the

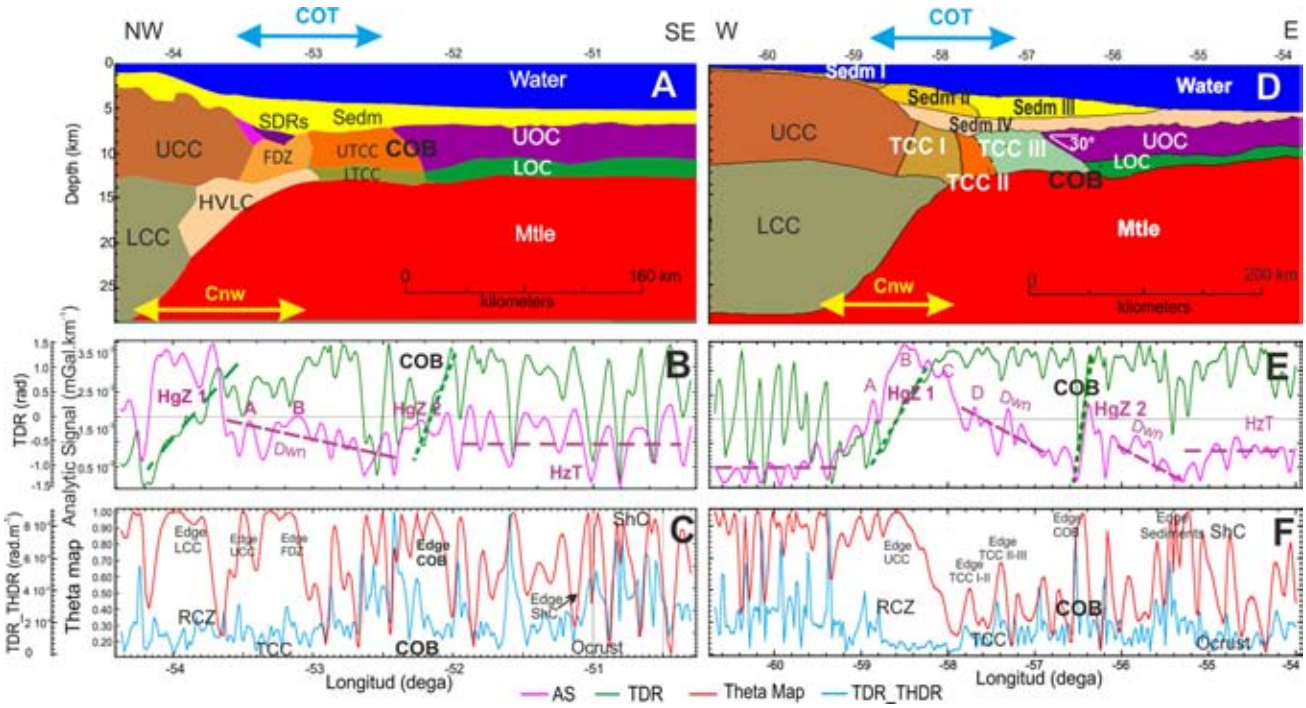

Figure 7. Models and enhancement techniques. The location of the COB is consistent with the models and techniques. (A) 2-D gravimetric model of Profile I; (B) analytic signal and tilt angle (TDR) (Profile I); (C) Theta map and tilt total horizontal derivative (TDR_THDR) (Profile I); (D) 2-D gravimetric model of Profile II; (E) analytic signal and Theta map (Profile II); (F) tilt angle and tilt total horizontal derivative (Profile II). COT, continent ocean transition; COB, continental–oceanic boundary; Sedm, sediments; SDRs, seaward-dipping reflectors; UCC, upper continental crust; LCC, lower continental crust; HVLC, high-velocity lower crust; FDZ, feeding dykes zone; UTCC, upper transitional continental crust; LTCC, lower transitional continental crust; UOC, upper ocean crust; LOC, lower ocean crust; Cnw, crustal narrowing; Mtle, mantle; HgZ 1, 2, Highest Zone 1, 2; Dwn, downward; HzT, horizontal trend, RCZ, regional contact zone; TCC I, transitional continental crust I; TCC II, transitional continental crust II; TCC III, transitional continental crust III; ShC, shallow contact; Ocrust, oceanic crust.

alignment of the maximum amplitude of $|AS(x, y)|$ (Fig. 3A); however, over the shear margin, the alignment of the maximum amplitude is subparallel to the Malvinas Fracture Zone; these changes of direction were assumed to be related to the mechanics of the breakup of Gondwana. The profiles A, B, C, D and E (Fig. 3A) have their maximum on the western side of the SDR series and, moreover, it is known that the SDR series are located in the continental crust within the continental–oceanic crust transition zone (Franke *et al.* 2007; Franke 2013), so the alignment of maxima shows the western side of the continental–oceanic crust transition. Profile E, which is transversal to SHM (shear margin) has its greatest amplitude at the base of the escarpment or the foot of the slope (Fig. 3A), and a shorter wavelength than the VPM (volcanic passive margin); the shear margin crustal edge is assumed as sharp and well defined due to the fact that in the formation process for this margin, shear tectonic control (developed at the first stage of the genesis of this transform margin), dominated. These results agree with of Rabinowitz & LaBrecque (1979), Lorenzo & Wessel (1997) and Bird & Hall (2009).

The result of applying the total horizontal derivative of the tilt angle (TDR_THDR) to the Bouguer anomalies can be seen in the map in Fig. 4B. This map differentiates three major areas: a westward one corresponding to the continental crust with warm colours, a second corresponding to the COT with cold colours in the centre, and finally a third to the east, corresponding to the oceanic crust with warm colours. In contrast to the result of the tilt angle, this technique emphasizes more superficial contacts or edges not revealed by tilt, enabling the interpretation of the Tandil and Rawson basement highs described by Ramos (1996) or pre- and synrift graben described by Franke *et al.* (2007). This technique allows to discriminate the beginning of the oceanic crust which consists of three layers; the upper one is a thin layer of sediment, the intermediate layer is constituted by pillowed textured basalts and dike swarms, and the bottom layer constituted by gabbros, dikes on top, metamorphosed mafic rocks and stratified peridotite accumulations in the base (Llambías 2008). The predominance of the signal's high frequencies shows the deformation of structures and sites igneous bodies related stress distribution during seafloor spreading, seen in profiles A, B, C, D and E (Fig. 4B).

In the crustal thickness map, under the Salado and Colorado basins, a thinning of the continental crust of ∼22.5 km is observed (Fig. 5B), consistent with its aulacogenic nature (Ramos 1996) and respecting the geometric symmetry of the crustal attenuation mentioned in Section 4.3.1. West of the Malvinas Islands, in the Malvinas Plateau, thinning of the continental crust can be observed under the East Malvinas Basin, showing thicknesses ranging from 12 to 16 km. The model warns of some correlation with the increase of crustal thickness in the areas of structural highs of Martín García, Tandil and Rawson. In order to discriminate the beginning of oceanic crust from the transition crust, an isopach curve of 6 km (Fig. 5B) was plotted by fixing the eastern edge of the crust.

Fig. 7 shows gravimetric 2-D models proposed in Section 4.4 representing structures comprising the continental margin and below enhancement-techniques profiles according to Section 4.2 in Profile I and Profile II (Fig. 5B). These enhancement techniques provided the determination of the COB by indicating contacts through maximum or conspicuous signals and finally allowing the determination of the boundary in a series of transverse profiles in a parallel

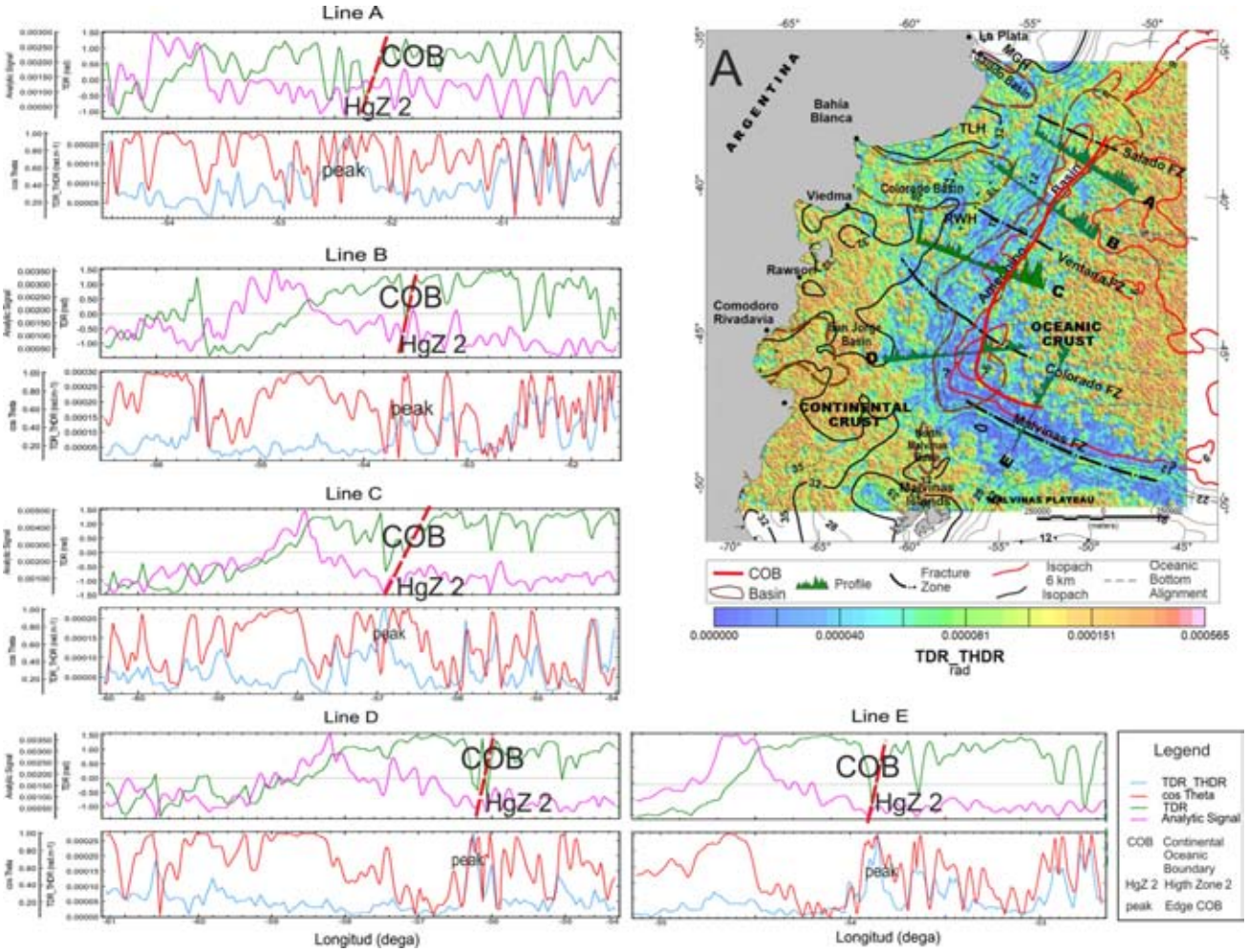

Figure 8. (A) Map of the location of the COB (red line) and the isopach crust–mantle discontinuity on the grid of the total horizontal derivative of the tilt angle. Lines A, B, C, D and E: Transverse profiles of the analytic signal, Theta map, tilt angle and total horizontal derivative of tilt. COB interpretation is indicated in lines A, B, C, D and E with the red line. The location of lines A, B, C, D and E is shown in panel (A).

line to the margin as result of an integration of the individual COB's profiles (Fig. 8A).

Continental–oceanic crust boundary (COB) Profile I (see location in Fig. 5A) corresponds to the contact between the upper transitional continental crust and the upper ocean crust; that is, in the middle of the attenuated transitional continental crust and the basaltic crust, at ∼52.5°W of longitude (see Fig. 7A). This is located east of the COT and crustal narrowing (Cnw), at the western end of the oceanic crust, where it reaches typical oceanic crust values (6 km).

In Fig. 7B two analytic signal maxima (magenta line) are shown as Highest Zone 1 (HgZ 1) and Highest Zone 2 (HgZ 2), a zone of downward linear trend (Dwn) and a horizontal trend (HzT). HgZ 1 is of wider amplitude than HgZ 2 and both exhibit low frequency, indicating deep contacts and a large density contrast, HgZ 1 being deeper than HgZ 2.

HgZ 1 was interpreted as indicating a contact between bodies in the lower continental crust (LCC) and HVLC, since it is deep with high density contrast, while the maximum limit HgZ 2 represents the COB (Fig. 7B), corresponding to the contact between the upper transitional continental crust (UTCC) and the upper oceanic crust (UOC) (Fig. 7A), since it is a relatively deep contact with high density contrast.

Dwn (Fig. 7B) is characterized by high frequency and low amplitudes, corresponding to surface contacts on the transitional continental crust. Dwn, contacts between feeding dikes zones (FDZ) and the upper continental crust (UCC) and between feeding dikes zone and the UTCC) are distinguished (peaks A and B, in magenta, respectively). These contrasts are reinforced by the valleys close to zero in tilt (green line in Fig. 7B) and by peaks in the horizontal derivative of the tilt angle (cyan line, Fig. 7C).

Contact between the LCC and HVLC causes a regional influence on tilt (dashed green line, Fig. 7B), denoted as the regional contact zone (RCZ) (dashed green line); however, the COB represents a more superficial contact and causes local dominance, making the zero crossing of tilt as displayed with a steep slope (green dotted line) and confirming a less superficial condition.

The horizontal regional trend zone (HzT) (magenta horizontal line, Fig. 7B) was interpreted as representing the response of the oceanic crust (OCrust) through the large number of peaks representing contacts between intrusions of magmatic material, fractures or shallow contacts (ShC) produced during seafloor spreading (Fig. 7C); these contacts are manifested in the tilt profile, which exhibits abundant zero crossings, showing maximum amplitudes in the Theta map (red line, Fig. 7C) and the tilt total horizontal derivative.

Another method that reinforces the interpretation of the COB location is the crustal thickness calculated according to eq. (11) (*Basement depth − Discontinuity Moho depth*), which Discontinuity Moho depth surface was obtain by gravimetric inversion (see Section 4.3.1); in especial the thickness of 6 km, that indicates the typical oceanic crust thickness (see Section 3.3) reinforces the COB location. The depth's crust–mantle discontinuity found by seismic refraction and reflection data were contrasted with those calculated by gravimetric inversion (see Table 1). The differences were considered satisfactory since they yielded root mean square (RMS) values between 1.7 and 2.9 km (refraction) and between 0.9 and 2.3 km (reflection). The biggest differences are concentrated 2.9 km under continental crust where the average crustal thickness reaches ∼27 km, and less than 1 km (0.9 km) under oceanic crust; the capture periods of both seismic refraction and reflection were also evaluated, the differences calculated between the modern captures of BGR 1998 and COPLA 2001–2002 (Franke *et al.* 2007, 2010; Schnabel *et al.* 2008) show a maximum RMS of 1.2 km against a 2.9 km maximum RMS over the oldest records (1963–1971). Thus, the depth of the crust–mantle discontinuity is sufficiently accurate to be extrapolated to the entire study region. The discrepancies were assumed to be due to lateral variations in density, principally HVLC, possessing velocity/densities similar to those of the top mantle.

A similar analysis was performed south of the Colorado Fracture Zone in Profile II (see location in Fig. 5A). The COB corresponds to the contact between the attenuated transition continental crust III (TCC III) and basaltic upper oceanic crust (UOC) located ∼ 56.4°W of longitude (Fig. 7D), which is east of the crustal narrowing (Cnw), on the eastern extreme of the continental–oceanic crust transition, where the narrowing of the transitional crust reaches typical oceanic crust values (6 km) and presenting a dip angle with relation to the horizontal axis ∼30°.

In Fig. 7B the analytic signal profile (magenta line), two maxima, HgZ 1 and HgZ 2 (Fig. 7E), two downward linear trend zones (Dwn 1 and Dwn 2) and a horizontal zone (HgZ) are presented.

Similarly, as in the Profile I analysis, HgZ 1 has amplitude larger than HgZ 2 and both are of low frequency, indicating deep contacts and great density contrast; HgZ 1 is deeper than HgZ 2. The HgZ 1 represents the contact between the LCC and the mantle (Mtle), being deep and of high density contrast. The maximum HgZ 2 represents the COB (Fig. 6E), that is to say, the TCC III–OCrust contact (Fig. 7D), since it is a relatively deep contact with high density contrast.

The peaks A, B, C and D in AS (magenta line) (Fig. 7E), which are of lower amplitude and greater frequency mounted on HgZ1 reveal superficial contacts, with sediments of different characteristics, Sedim I with Sedim II in line A, the UCC with transitional continental crust I (TCC I) in B, TCC I with transitional continental crust II (TCC II) in C, and sediments with different characteristics (Sedim II and Sedim III) in peak D.

The horizontal regional trend zone line (HzT, magenta dashed horizontal), similarly to Profile I, was interpreted as the response to the oceanic crust (OCrust) due to magmatic material intrusions or volcanism starting in the basement and fractures produced by seafloor spreading (Fig. 7D); these shallow contacts (ShC) are manifested in tilt exhibiting abundant zero crossings and the horizontal derivative of the tilt angle showing maximum amplitudes (Fig. 7F).

Moreover, the contact between LCC and Mtle causes regional influence in tilt (green line), denoted as a regional contact zone (RCZ), and influences tilt so that zero crossing occurs with a slope of low gradient (dashed green line, Fig. 6E); however, shallower COB causes local preponderance, so that the zero crossings of tilt exhibit greater slope (green line points), confirming its superficial condition (Fig. 7E).

Modelling represented an important asset, because apart from determining the location of the COB, it allowed us to understand the architecture the margin by finding that the continental–oceanic crust transition has different characteristics north and south of the Colorado Fracture Zone. To the north it is characterized by a narrowing of the crust from west to east of 30 to 6 km along approximately 160 km, and also by the gradual variation of densities from top to bottom and from west to east, according to Airy isostatic passive-margin compensation (Introcaso 2003).

Similar results obtained above, transverse profiles to the Argentine continental margins (only five lines A, B, C, D and E) are presented in order to show the application to each of them of enhancement techniques for locating the COB reinforced by the 6 km crustal thickness (Fig. 8A).

6 DISCUSSION

One of the most distinctive characteristics of free-air anomalies is the 'edge effect' (Worzel & Shurbet 1955; Watts & Fairhead 1999; Stewart *et al.* 2000), in the continental margins; edge effect appears as a visible feature in the Argentine continental margin. The north section of the Colorado Fracture Zone runs from 35°S to 43°S in a northeasterly direction, presenting a 'maximum' (warm colours) on the edge of the shelf, a 'minimum' (cold colours) on the continental slope emersion and a slope and rise on the region of greater sediment thickness. The section south of the Colorado Fracture Zone runs from 43°S to 47°S northwards, where two maximum and two minimum values are seen between the shelf and the abyssal plain (Fig. 1A).

In the shear margin, the edge effect runs predominantly in an east–west direction on the Malvinas Escarpment, presenting a maximum on the edge of the Malvinas Plateau and a minimum at the base of the escarpment (Fig. 1A). The edge effect in this continental margin is of greater amplitude and frequency than in the exposed VPM; the largest amplitude is due to the slope (>2000 m) of the Malvinas Escarpment, and the largest frequency is due to the abrupt transition northwards from continental crust (Malvinas Plateau) to oceanic crust.

Significant positive anomalies over the Colorado and Salado basins allow their interpretation as aulacogenic basins. This high positive Bouguer anomaly, as shown in Fig. 2, is attributed by Introcaso & Ramos (1984) and Introcaso (1990, 2003) to a dominant isostatic overcompensation; that is to say, to an excessively thinned crust beneath the basin.

Many studies of the continental margin take place in the first kilometres of depth, that is, they focus on the sedimentary basins of the continental shelf (Ewing *et al.* 1963, 1964, 1971; Ludwig *et al.* 1968, 1978, 1979; Lonardi & Ewing 1971), the transient volcanism emplacement (Gladczenko *et al.* 1997; Hinz *et al.* 1999; Franke *et al.* 2007, 2010) or it economic potential in terms of the exploitation of natural resources (Urien & Zambrano 1970, 1996; Urien 2001). COB has been studied from the gravimetric and magnetic fields by LaBrecque & Rabinowitz (1979) and Dragoi-Stavar & Hall (2009); and also including seismic data by Hinz *et al.* (1999) Franke *et al.* (2007), Schnabel *et al.* (2008) or Blaich *et al.* (2009). In order to improve the study and characterization of the COB, it was proposed to add the modelling of a Moho with a strong control on their location through new seismic data (2001–2002) from COPLA.

Bathymetric and gravimetric data from satellite altimetry were validated based on COPLA surveys data (see Section 3.1). Furthermore we have made a sensitivity analysis to study how a variation in bathymetric model would affect the results of the enhancement techniques and inversion. It turns out that a variation of ±100 m in bathymetry is reflected in a variation of ±5.6 mGal in Bouguer anomalies while shifts in the bathymetry larger than 500 m produce an effect of ±28 mGal. As we stated above, in Section 3.2, over 500 m of depth variations occur at particular locations with specific characteristics such as steep slopes, submarines canyons or small terraces guns, which are located outside the area of the COB. Because almost the entire study area is in the range ±100 m, then the accuracy of satellite altimetry data was considered as sufficient to apply enhancement techniques.

The edge effect shows the sensitivity of free-air anomalies to the seafloor topography, confirmed by the location of maxima and minima correlated with variation in the deep seafloor. However, free-air anomalies include, principally, information related to the structures comprising the top crust. In order to extract information from the lower crust, topographical and geological corrections of Bouguer anomalies were calculated.

The results of the application of the AS gave two maximum (HgZ 1 and HgZ 2, Figs 7B and E), indicating greater contact with transition continental crust, that is, the beginning of COT and less than the maximum indicated by the COB. The application of tilt clearly showed two contact points of big density contrast showed by the tangent line. One shows the contact between the continental crust and transition crust and the other the contact between the transition crust and the oceanic one, being these tangent lines, in the same place where the maximums HgZ 1 and HgZ 2 shown by the AS. Theta map and Total Horizontal Derivative of Tilt collaborate in the interpretation, which behave like an automatic gain control filter and tend to equalize the output amplitude of gravimetric anomalies across a grid (Verduzco *et al.* 2004), being consistent with the maximums and with the horizontal line of the AS, where crystalline basement is horizontal.

The Theta map can help determine the COB by discriminating contacts, with better definition than that provided by the tilt. The edges are detected, even with dipping, while the amplitude of the analytic signal does not capture these characteristics (Wijns *et al.* 2005). Franke *et al.* (2007) describe three series of SDRs with the western wedges being thicker. The location of the contacts of the main wedges is shown on the Theta map by alignment of maxima with warm colours parallel to the location of said wedges (Fig. 4A).

Crustal thickness reflects the nature of the crust, that is, the compensated continental crust has a thickness of ∼40 to 30 km (Introcaso *et al.* 2003; Franke *et al.* 2007; Bai *et al.* 2014), while the thickness of the oceanic crust on average is ∼7 ± 0.8 km, with extreme limits of 5.0 to 8.5 km, according to White *et al.* (1992). The seabed is covered by sediments which were not considered part of the crustal thickness in this work. The crustal thickness in the continental margin varies between typical continental and ocean thicknesses values ∼30–20 km. By seismic refraction-reflection surveys, isolated and scattered, thickness was recorded, in order to obtain the isopach 6 km and a regional grid was necessary to be made.

Previous studies in the Colorado Basin utilized seismic recordings of the continental crust by BGR with ocean-bottom hydrophones, obtaining a result of ∼30 km thickness (Franke *et al.* 2006); in earlier gravimetric surveys in the basin, a thickness of ∼28 km was registered (Introcaso *et al.* 2003). Moreover, studies performed in the continental shelf at 44°S and in the continental–oceanic crust transition showed that crustal thickness varies from ∼25 to 14 km from west to east (Schnabel *et al.* 2008). In addition, the global average crustal thickness of igneous oceanic crust away from anomalous regions such as Fracture Zones and hot spots is ∼7 ± 0.8 km, with extreme limits of 5.0–8.5 km, according to White *et al.* (1992). Based on the above considerations, in this study, the 6 km isopach line supports the determination of the edge of the transition crust.

This new crustal thickness model of the Argentine sea (see Section 4.3.2) showed a clear differentiation between VPM and SHM, clearly discriminates main characteristic, the continental crust from the ocean crust, and the gradient in the transition region, the crustal attenuation under the sedimentary Salado, Colorado, San Jorge and Malvinas basins; and this new crustal thickness model of the Argentine is sensitive to the Malvinas, Colorado, Ventana and Salado Fracture Zones. In addition, the new model of crustal thickness presents higher resolution (5 × 5 arcmin cell-size).

Previous works were improved by introducing a new crustal thickness model based on inversion and of the AB_{CG} at 30 km of upward continuation (AMGI). Uniqueness of inversion and separation of the gravitational field in order to obtain Moho's depth has been solved after imposing seismic data as constraints, such as seismic information and the density contrast according to Hinze *et al.* (2005), and by means of geophysics and geologic data. There are good regional seismological models in South America such as Assumpção *et al.* (2013) or Chulick *et al.* (2013), data about the South Atlantic Ocean, but they do not have the same quantity of seismic data as COPLA and BGR on the Argentine Sea. From new and recent seismic survey data recorded by COPLA, the regional Moho depth by inversion was adjusted and contrasted, thus improving proposed gravity models and regional seismological models.

Regarding the differences between our model, AMGI, and the models based on gravity, it was note that VMM (Bagherbandi *et al.* 2013) and GMSA12 (van der Meijde *et al.* 2015) have presented small differences, that is, RMS 2.4 km, mean values −4.6 and −4.5 km, respectively, and the differences with the seismological models, that is, 'Seismic structure of South America' (Chulick *et al.* 2013) is the model that presented less differences (Table 2). It should be said that Bagherbandi *et al.* (2013), Reguzzoni & Sampietro (2015), and van der Meijde *et al.* (2013) performs equally well (i.e. RMS 2.4 or 2.8 and mean of 4.1 or 4.6). It is also interesting to note that all the models show a negative mean difference; it was assumed that the trend is due to the difference in scale models, while the GEMMA (Reguzzoni & Sampietro 2015), VMM (Bagherbandi *et al.* 2013), and CRUST1.0 (Laske *et al.* 2013) are global models, AMGI is a local model. This is repeated with the South American models DMM (van der Meijde *et al.* 2015), and Seismic structure of South America (Chulick *et al.* 2013) reaching mean of −0.6 km and −1.4 km respectively.

From a purely mathematical point of view, there is always more than one model that will reproduce the observed data to the same degree of accuracy (the so-called non-uniqueness problem). However, geologic units producing the gravimetric data that was acquired in real-world problems do not have an arbitrary variability. Imposing simple constraints and restrictions on admissible solutions from geologic knowledge and its integration with independent data sets leads usually to robust results. Contrasting previous studies of crustal thickness gave acceptable results (Nabighian *et al.* 2005). The seismic reflection lines were converted to depth according to Ludwig *et al.* (1978) and then they were interpreted in order to be integrated to the constraints of gravity models and to

minimize the effects of ambiguity when inverting the gravitational field.

Modelling represented an important asset, because apart from determining the location of the COB, it allowed us to understand the architecture of the margin, and to find out that the continental–oceanic crust transition has different characteristics north and south of the Colorado Fracture Zone. To the north it is characterized by a narrowing of the crust from west to east of 30 to 6 km along approximately 160 km, a gradual development of densities from top to bottom and from west to east, according to its own Airy isostatic passive-margin compensation (Fig. 6). To the south, on the other hand, there is no HVLC or sediment-control edge effect. However, in both margin kind, it could be found a progressive increase in density from top to bottom and from west to east, according to of the isostatic compensation of the passive margins.

Gravity data can be linked to seismic attributes since they can help define/estimate the physical properties of the source structure causing the anomaly (Verduzco *et al.* 2004). These models have been constrained with available seismic data, and geologic information (Hinz *et al.* 1999; Franke *et al.* 2002, 2007, 2010; Schnabel *et al.* 2008). Therefore, 2-D gravimetric modelling was applied along two profiles perpendicular to the margin in order to validate the crustal thinning and the COB. According to Pawlowski (2008) on considering that analysis of gravity anomaly data can be an efficient and economical way to delineate the world's offshore continental margins. The COB was then determined in profiles by applying these methods, and then extrapolated to the entire continental margin (Fig. 8A).

7 CONCLUSIONS

The method presented, based on a combination of enhancement techniques, crustal thickness and 2-D gravimetric modelling, allows rapid identification of the COB in rift VPMs (volcanic passive margin) over large areas, such as the Argentine continental margin. Enhancement techniques were calculated from Bouguer anomalies corrected by sediment thickness. Crustal thickness was derived as the difference between the depths of the interpreted crystalline basement and the crust–mantle discontinuity, and these 2-D and 3-D gravimetric models were constrained using seismic data.

The enhancement techniques used were the analytic signal, Theta map, tilt angle and horizontal derivative of the tilt; these have proven effective in determining deep contacts and, with the horizontal derivative of the tilt angle, for shallow contacts also. These techniques allowed determination of the location of the COB on profiles transverse to the continental margin and differentiation of deep contacts through the AS (analytical signal) frequency and wavelength or the slope of the tilt angle tangent line.

The calculation of crust–mantle discontinuity depth required obtaining a regional gravimetric field in order to perform the gravimetric inversion in the frequency domain; the most suitable regional gravimetric field was produced by Bouguer anomalies corrected by sedimentary effects and by upward continuation through 35 km. The depth of the discontinuity obtained was convenient as it could be compared with scattered sections of multichannel seismic reflection and wide-angle seismic refraction conducted at different times in the Argentine continental margin; the result of the comparison yielded RMS of 1.2 km.

Application of the gravimetric method determined a transition crust characterized by a crustal narrowing with thicknesses varying from ∼29 to ∼6 km according to worldwide results, and by the composition of an attenuated continental crust with abundant magmatic material intrusion being reflected in the lateral variation in density of the transition structures.

These results agree with previous studies conducted in the margin region based on seismic methods, which show a continental crust thickness of 30 km, ∼5 km of oceanic crust and the presence of HVLC (e.g. Schnabel *et al.* 2008). The most of the thinning process is produced in the transition continental–oceanic crust in which the SDRs, the greater sediment thickness and part of the HVLC to the north of the Colorado Fracture Zone are located.

The crust–mantle discontinuity depth, seismic interpretations HVLC, SDRs, the sediment thickness and ocean bottom, used as a limiting surfaces, allowed carry out 2-D modelling to estimate density of the superstructures as continental, transitional and oceanic crusts.

The validation and effectiveness of the methodology on profiles allowed extrapolation to the entire continental margin by locating the COB with enhancement techniques together with a 6 km isopach for crustal thickness of oceanic crust. Finally, the conditions in the profiles were checked in order to extrapolate them to the entire continental margin and integrate them in a line parallel to the margin.

Both north and south of the Colorado Fracture Zone, the techniques used in the gravimetric method were consistent and coherent with each other, so it can be affirmed that the gravimetric method with the support of seismic data can be used to determine continental margins with similar characteristics to the Argentine margins.

ACKNOWLEDGEMENTS

This work was partially performed through María Alejandra Arecco's research project for the 'Comisión Nacional del Límite Exterior de la Plataforma Continental' (COPLA), financed by projects PNUD ARG 06/018, PNUD ARG 10/009 and PICT 2012/2716 ANPCYT (Argentina). The authors thank two anonymous reviewers for their helpful comments on the original manuscript and would like to thank COPLA (Argentina) and BGR (Germany) for permission to use compressional wave velocity data, crystalline basement multichannel seismic interpretations, sediment thickness, bathymetric and databases.

REFERENCES

Amante, C. & Eakins, B.W., 2009. ETOPO1 1 Arc-Minute Global Relief Model Procedures, Data Sources and Analysis, NOAA Technical Memorandum NESDIS NGDC-24, National Geophysical Data Center, NOAA, doi:10.7289/V5C8276M.

Assumpção, M., Feng, M., Tassara, A. & Julià, J., 2013. Models of crustal thickness for South America from seismic refraction, receiver functions and surface wave tomography, *Tectonophysics,* **609,** 82–96.

Austin, J.A. & Uchupi, E., 1982. Continental-Oceanic crustal transition of southwest Africa, *AAPG Bull.,* **66,** 1328–1347.

Arecco, M.A., Pizarro, G. & Ruiz, F., 2014. Aplicación del método gravimétrico en el margen argentino, *Geoacta,* **39**(1), 25–34.

Bagherbandi, M., Tenzer, R., Sjöberg, L.E. & Novák, P., 2013. Improved global crustal thickness modeling based on the VMM isostatic model and non-isostatic gravity correction, *J. Geodyn.,* **66,** 25–37.

Bai, Y., Williams, S.E., Müller, R.D., Liu, Z. & Hosseinpour, M., 2014. Mapping crustal thickness using marine gravity data: methods and uncertainties, *Geophysics,* **79**(2), G27–G36.

Barker, P.F., 1979. The history of ridge-crest offset at the Falkland–Agulhas Fracture Zone from a small-circle geophysical profile, *Geophys. J. R. astr. Soc.,* **59,** 131–145.

Ben-Avraham, Z., Hartnady, C.J.H. & Kitchin, K.A. 1997. Structure and tectonics of the Agulhas-Falkland Fracture Zone, *Tectonophysics,* **282,** 83–98.

Ben-Avraham, Z., Hartnady, C.J.H. & Malan, J.A. 1993. Early tectonic extension between the Agulhas Bank and the Falkland Plateau due to the rotation of the Lafonia microplate, *Earth planet. Sci. Lett.,* **117,** 43–58.

Bird, D., 2001. Shear margins: continent-ocean transform and fracture zone boundaries, *Leading Edge,* **20,** 150–159.

Bird, D.E. & Hall, S.A., 2009. Central South Atlantic kinematics: a 3D ocean basin-scale model of the Walvis Ridge and Rio Grande Rise, *EOS, Trans., Am. geophys. Un.,* Fall Meeting Supplement, 90, T51A-1487.

Blaich, O., Faleide, J.I., Tsikalas, F., Franke, D. & León, E., 2009. Crustal-scale architecture and segmentation of the Argentine margin and its conjugate off South Africa, *Geophys. J. Int.,* **178,** 85–105.

Blaich, O.A., Faleide, J.I. & Tsikalas, F., 2011. Crustal breakup and continent-ocean transition at South Atlantic conjugate margins, *J. geophys. Res.,* **116,** B01402, doi:10.1029/2010JB007686.

Brocher, T.M., 2005. Empirical relations between elastic wavespeeds and density in the Earth's crust, *Bull. seism. Soc. Am.,* **95,** 2081–2092.

Caratori Tontini, F., Cocchi, L. & Carmisciano, C., 2008. Potential field inversion for a layer with uneven thickness: the Tyrrhenian Sea density model, *Phys. Earth planet. Inter.,* **166,** 105–111.

Christensen, N.I. & Mooney, W.D., 1995. Seismic velocity structure and composition of the continental crust: a global view, *J. geophys. Res.,* **100,** 9761–9788.

Chulick, G.S., Detweiler, S. & Mooney, W.D., 2013. Seismic structure of the crust and uppermost mantle of South America and surrounding oceanic basins, *J. South Amer. Earth Sci.,* **42,** 260–276.

Cooper, G.R.J., 2009. Enhancing circular features in potential field data using a generalized radial derivative filter, in *11th SAGA Biennial Technical Meeting and Exhibition*, *Abstract,* pp. 273–275, SAGA.

Cooper, G.R.J. & Cowan, D.R., 2006. Enhancing potential field data using filters based on the local phase, *Comput. Geosci.,* **32,** 1585–1591.

Dahl-Jensen, T., Holbrook, W.S., Hopper, J.R., Kelemen, P.B., Larsen, H.C., Detrick, R., Bernstein, S. & Kent, G., 1997. Seismic investigation of the east Greenland volcanic rifted margin, *Geol. Greenl. Surv. Bull.,* **176,** 50–54.

Dean, W., 1958. Frequency analysis for gravity and magnetic interpretation, *Geophysics,* **23,** 97–122.

Dragoi-Stavar, D. & Hall, S., 2009. Gravity modeling of the ocean-continent transition along the South Atlantic margins, *J. geophys. Res.,* **114,** B09401, doi:10.1029/2008JB006014.

Eldholm, O., Skogseid, J., Planke, S. & Gladczenko, T.P., 1995. Volcanic margin concepts, in *Rifted Ocean–Continent Boundaries*, pp. 1–16, eds Banda, E., Torné, M. & Talwani, M., NATO ASI Series, Kluwer Academic Publishers.

Ewing, M., Ludwig, W.J. & Ewing, J.I., 1963. Geophysical investigations in the submerged Argentine coastal plain. Part 1. Buenos Aires to Peninsula Valdez, *Bull. geol. Soc. Am.,* **74,** 275–292.

Ewing, M., Ludwig, W.J. & Ewing, J.I., 1964. Sediment distribution in the oceans: the Argentine Basin, *J. geophys. Res.,* **69**(10), 2003–2032.

Ewing, J.I., Ludwig, W.J., Ewing, M. & Eittrem, S.L., 1971. Structure of Scotia Sea, Falkland/Malvinas Plateau, *J. geophys. Res.,* **76**(29), 7118–7137.

Franke, D., 2013. Rifting, lithosphere breakup and volcanism: comparison of magma-poor and volcanic rifted margins, *Mar. Pet. Geol.,* **43,** 63–87.

Franke, D., Neben, S., Hinz, K., Meyer, H. & Schreckenberger, B., 2002. Deep crustal structure of the argentine continental margin from seismic wide-angle and multichannel reflection seismic data, in *AAPG Hedberg Conference* 'Hydrocarbon Habitat of Volcanic Rifted Passive Margins', September 8–11, 2002, Stavanger, Norway.

Franke, D., Neben, S., Schreckenberger, B., Schulze, A., Stiller, M. & Krawczyk, C.M., 2006. Crustal structure across the Colorado Basin, offshore Argentina, *Geophys. J. Int.,* **165,** 850–864.

Franke, D., Neben, S., Ladage, S., Schreckenberger, B. & Hinz, K., 2007. Margin segmentation and volcano-tectonic architecture along the volcanic margin off Argentina/Uruguay, South Atlantic, *Mar. Geol.,* **244,** 46–67.

Franke, D. *et al.*, 2010. Birth of a volcanic margin off Argentina, South Atlantic, *Geochem. Geophys. Geosyst.,* **11**(2), Q0AB04, doi:10.1029/2009GC002715.

Gardner, G.H.F., Gardner, L.W. & Gregory, A.R., 1974. Formation velocity and density—the diagnostic basics for stratigraphic traps, *Geophysics,* **39,** 770–780.

Ghidella, M.E., Köhn, J. & Gianibelli, J.C., 2002. Low altitude magnetic anomaly compilation in Argentine: its comparition with satellite data, *American Geophysical Union,* Spring Meeting, http://www.dsri.dk/multimagsatellites/.

Gladczenko, T.P., Hinz, K., Eldholm, O., Meyer, H., Neben, S. & Skogseid, J., 1997. South Atlantic volcanic margins, *J. Geol. Soc. Lond.,* **154,** 465–470.

Guo, L., Meng, X., Chen, Z., Li, S. & Zheng, Y., 2013. Preferential filtering for gravity anomaly separation, *Comput. Geosci.,* **51,** 247–254.

Hansen, R.O., Pawlowski, R.S. & Wang, X., 1987. Joint use of analytic signal and amplitude of horizontal gradient maxima for three-dimensional gravity data interpretation, in *57th Annual International Meeting SEG*, New Orleans, Expanded Abstracts, 100–102.

Hinz, K., Neben, S., Schreckenberger, B., Roeser, H., Block, M., Goncalves De Souza, K. & Meyer, H., 1999. The Argentine continental margin north of 48ºS: sedimentary successions, volcanic activity during breakup, *Mar. Pet. Geol.,* **16,** 1–25.

Hinze, W.J. *et al.*, 2005. New standards for reducing gravity data: The North American gravity database, *Geophysics,* **70,** J25–J32.

Hofmann-Wellenhof, B. & Morritz, H., 2006. *Physical Geodesy,* pp. 404, Springer.

Introcaso, A., 1990. Studies of aulacogenic Salado and Colorado in Argentina by means of gravity data, *Ed. South American Gravity Project,* Final Meeting (Quito), 1–9.

Introcaso, A., 2003. Significativa descompensación isostática en la Cuenca del Colorado (República Argentina), *Revista de la Asociación Geológica Argentina,* **58,** 474–478.

Introcaso, A. & Ramos, V.A., 1984. La cuenca del Salado: un modelo de evolución aulacogénica, in *IX° Congreso Geológico Argentino Actas,* vol. 3, pp. 27–46, San Carlos de Bariloche, Argentina.

Introcaso, A., Ghidella, M.E., Ruiz, F., Crovetto, C.B., Introcaso, B. & Paterlini, C.M., 2003. Métodos gravi-magnetométricos modernos para analizar las características estructurales de la plataforma continental argentina, *Geoacta,* **33,** 1–20.

Jackson, M.P.A., Cramez, C. & Fonck, J.M., 2000. Role of subaerial volcanic rocks and mantle plumes in creation of South Atlantic margins: implications for salt tectonics and source rocks, *Mar. Pet. Geo.,* **17,** 477–498.

Kane, M.F., 1962. A comprehensive system of terrain corrections using a digital computer, *Geophysics,* **27,** 455–462.

Korenaga, J., Holbrook, W.S., Detrick, R.S. & Kelemen, P.B., 2001. Gravity anomalies and crustal structure at the southeast Greenland margin, *J. geophys. Res.,* **106,** 8853–8870.

Kowsmann, R., Leyden, R. & Francisconi, O., 1977. Marine Seismic Investigations, Southern Brazil Margin, *Am. Assoc. Pet. Geol. Bull.,* **61,** 546–557.

Lafehr, T.R., 1991. Standardization in gravity reduction, *Geophysics,* **56**(8), 1170–1178.

Laske, G., Masters, G., Ma, Z. & Pasyanos, M., 2013. Update on CRUST1.0 - A 1-degree Global Model of Earth's Crust, *Geophys. Res. Abstracts,* Vol. 15, EGU General Assembly 2013, EGU2013-2658.

Leyden, R., Ludwig, W.J. & Ewing, M., 1971. Structure of Continental Margin off Punta del Este, Uruguay, and Río de Janeiro, Brazil, *Am. Assoc. Pet. Geol. Bull.,* **55**(12), 2161–2173.

Lince Klinger, F., Martínez, P., Rapalini, A.E., Giménez, M.E., López De Luchi, M.G., Croce, F.A. & Ruiz, F., 2010. Modelo gravimétrico en el borde noreste del macizo norpatagónico, *Revista Brasileira de Geofísica,* **28**(3), 463–472.

Lister, G.S., Etheridge, M.A. & Symonds, P.A., 1986. Detachment faulting and the evolution of passive continental margins, *Geology,* **14,** 246–250.

Llambías, E., 2008. *Geología de los cuerpos ígneos,* Serie B, Didáctica y Complementaria 29 e INSUGEO, Serie Correlación Geológica 15*,* pp. 1–222, Asociación Geológica Argentina.

Lonardi, A.G. & Ewing, M., 1971. Sediment transport and distribution in the Argentine Basin. 4. Bathymetry of the continental margin, Argentine Basin and other related provinces. Canyons and Sources of Sediments, in *Physics and Chemistry of the Earth,* vol. 8, pp. 81–121, 1st edn., Pergamon Press.

Lorenzo, J.M. & Wessel, P., 1997. Flexure across a continent-ocean fracture zone: the northern Falkland/MalvinasPlateau, South Atlantic, *Geo-Mar. Lett.,* **17,** 110–118.

Ludwig, W., Carpenter, G., Houtz, R.E., Lonardi, A.G. & Rios, F.F., 1978. Argentine Continental Margin, *Sediment Isopach Map,* American Association of Petroleum Geologists.

Ludwig, W.J., Ewing, J.I. & Ewing, M., 1968. Structure of Argentine continental margin, *Am. Assoc. Pet. Geol. Bull.,* **52**(12), 2337–2368.

Ludwig, W.J., Ewing, J.I., Windish, C.C., Lonardi, A.g. & Rios, F.F., 1979. Structure of the Colorado Basin and continent ocean crust boundary off Bahia Blanca, Argentina, in *Geological and Geophysical Investigations of Continental Margins,* vol. 29, pp. 113–124, eds Watkins, J.S., Montadert, L. & Wood, P., American Association of Petroleum Geologists.

Menzies, M.A., Klemperer, S.L., Ebinger, C.J. & Baker, J., 2002. Characteristics of volcanic rifted margins, in *Volcanic Rifted Margins*, vol. 362, pp 1–14, eds Menzies, M.A., Klemperer, S.L., Ebinger, C.J. & Baker, J., Soc. Amer. Spl., Special Paper.

Miller, H.G. & Singh, V., 1994. Potential field tilt-A new concept for location of potential field sources, *J. Appl. Geophys.,* **32,** 213–217.

Mutter, J.C., Talwani, M. & Stoffa, P.L., 1982. Origin of seaward dipping reflectors in oceanic crust off the Norwegian margin by subaerial seafloor spreading, *Geology,* **10,** 353–357.

Nabighian, M.N., 1972. The analytic signal of two-dimensional magnetic bodies with polygonal cross section: its properties and use for automated interpretation, *Geophysics,* **37,** 507–517.

Nabighian, M.N., 1974. Additional comments on the analytic signal of two-dimensional magnetic bodies with polygonal cross section, *Geophysics,* **39,** 85–92.

Nabighian, M.N., 1984. Toward a three-dimensional automatic interpretation of potential field data via generalized Hilbert transforms: fundamental relations, *Geophysics,* **49,** 780–786.

Nabighian, M.N, Grauch, V.J.S., Li, Y., Peirce, J.W., Phillips, J.D. & Ruder, M.E., 2005. The historical development of the magnetic method in exploration, *Gehphysics,* **70,** 33ND–61ND.

Nagy, D., 1966. The gravitational attraction of a right rectangular prism, *Geophysics,* **31**(2), 362–371.

Neben, S. & Schreckenberger, B., 2005. Geophysical investigations offshore Argentine and Uruguay ARGURU, in *Cruise Report BGR04*, pp. 1–99, Bundesanstalt für Geowissenschaften und Rohstoffe, Hannover.

Pacino, M.C. 1989. Perfil gravimetrico transcontinental en la latitud 39 Sur. in *XII° Congreso Geológlco Argentino y II° Congreso de Exploraci6n de Hidrocarburos,* pp. 282–285, Actas III, Mendoza.

Pacino, M.C. & Introcaso, A., 1987. Regional anomaly determination using the upwards continuation method, *Bollettino di Geofisica Teorica ed Applicata,* **29**(114), 113–122.

Pankhurst, R., Rapela, C., Fanning, C. & Márquez, M., 2006. Gondwanide continental collision and the origin of Patagonia, *Earth Sci. Rev.,* **76,** 235–257.

Parker, R.L., 1972. The rapid calculation of potential anomalies, *Geophys. J. R. astr. Soc.,* **31,** 447–455.

Parker, R.L., 1975. The theory of ideal bodies for gravity interpretation, *Geophys. J. R. astr. Soc.,* **42,** 315–334.

Parker, R.L. & Huestis, S.P., 1974. The inversion of magnetic anomalies in the presence of topography, *J. geophys. Res.,* **79,** 1587–1593.

Parsiegla, N., Gohl, K. & Uenzelmann-Neben, G., 2007. Deep crustal structure of the sheared South African continental margin: first results of the Agulhas-Karoo Geoscience Transect, *South Afr. J. Geol.,* **110,** 393–406.

Pawlowski, R.S., 1995. Preferential continuation for potential-field anomaly enhancement, *Geophysics,* **60**(2), 390–398.

Pawlowski, R.S., 2008. The use of gravity anomaly data for offshore continental margin demarcation, *Leading Edge,* 772–727.

Rabinowitz, P.D. & LaBrecque, J., 1979. The Mesozoic South Atlantic Ocean and evolution of its continental margins, *J. geophys. Res.,* **84,** 5973–6002.

Ramos, V.A., 1996. Evolución tectónica de la Plataforma Continental, Geología y Recursos de la Plataforma Continental, in *Geología y Recursos Naturales de la Plataforma Continental Argentina,* pp 385–404, eds Ramos, V.A. & Turic, M.A., Relatorio XIII° Congreso Geológico Argentino y III° Congreso de Exploración de Hidrocarburos.

Ramos, V.A., 2008. Patagonia: a Paleozoic continental adrift?, *J. South Amer. Earth Sci.,* **26,** 235–251.

Reguzzoni, M. & Sampietro, D., 2015. GEMMA: an earth crustal model based on GOCE satellite data, *Int. J. Appl. Earth Obs. Geoinf.,* **35,** 31–43.

Reguzzoni, M., Sampietro, D. & Sansò, F., 2013. Global Moho from the combination of the CRUST2.0 model and GOCE data, *Geophys. J. Int.,***195** (1), 222–237.

Roest, W.R., Verhoef, J. & Pilkington, M., 1992. Magnetic interpretation using 3-D analytic signal, *Geophysics,* **57,** 116–125.

Rossi, L., 2013. Bayesian interpretation of gravity data with geological prior information, *Master graduation thesis*, *Politecnico di Milano*.

Rossi, L., Reguzzoni, M., Sampietro, D. & Sansò, F., 2015. Integrating geological prior information into the inverse gravimetric problem: the Bayesian approach, in *International Association of Geodesy Symposia,* pp. 1–8, Springer.

Ruiz, F. & Introcaso, A., 1999. Un modelo gravimétrico 3D de la profunda cuenca sedimentaria de Ischigualasto-Villa Unión (San Juan y La Rioja)-Argentina, *Rev. Bras. Geofís.,* **17,** 3–11.

Sampietro, D. & Sansò, F., 2012. Uniqueness theorems for inverse gravimetric problems, in *VII Hotine-Marussi Symposium on Mathematical Geodesy,* pp. 111–115, eds Sneeuw, N., Novák, P., Crespi, M. & Sansò, F. Springer.

Sandwell, D.T. & Smith, W.H.F., 1997. Marine gravity anomaly from Geosat and ERS 1 satellite altimetry, *J. geophys. Res.,* **102,** 10 039–10 054.

Sandwell, D.T. & Smith, W.H.F., 2001. Bathymetric estimation, in *Satellite Altimetry and Earth Sciences,* pp. 441–457, eds Fu, L.L. & Cazenave, A., Academic Press.

Sandwell, D.T. & Smith, W.H.F., 2009. Global marine gravity from retracked Geosat and ERS-1 altimetry: ridge segmentation versus spreading rate, *J. geophys. Res.,* **114,** B01411, doi:10.1029/2008JB006008.

Sandwell, D.T., Müller, R.D., Smith, W.H.F.,, Garcia, E. & Francis, R. 2014. New global marine gravity model from CryoSat-2 and Jason-1 reveals buried tectonic structure, *Science,* **346**(6205), 65–67.

Schnabel, M. *et al.*, 2008. The structure of the lower crust at the Argentine continental margin, South Atlantic at 44°S, *Tectonophysics,* **454,** 14–22.

Smith, W.H.F., 1993. On the accuracy of digital bathymetric data, *J. geophys. Res.,* **98,** 9591–9603.

Smith, W.H.F. & Sandwell, D.T., 1994. Bathimetric prediction from dense satellite altimetry and sparce shipboard bathymetry, *J. geophys. Res.,* **99,** 21 803–21 824.

Soto, M., Morales, E., Veroslavsky, G., de Santa Ana, H., Ucha, N. & Rodríguez, P., 2011. The continental margin of Uruguay: crustal architecture and segmentation, *Mar. Petrol. Geol.,* **28,** 1676–1689.

Stewart, J., Watts, A.B. & Bagguley, J.G., 2000. Three-dimensional subsidence analysis and gravity modelling of the continental margin offshore Namibia, *Geophys. J. Int.,* **141,** 724–746.

Talwani, M., Worzel, J.L. & Landisman, M., 1959. Rapid gravity computations for two-dimensional bodies with application to the Mendocino submarine fracture zone, *J. geophys. Res.,* **64**(1), 49–59.

Tarantola, A. & Valette, B., 1982. Inverse problem = Quest for information, *J. Geophys.,* **50**(3), 150–170.

Thurston, J.B. & Smith, R.S., 1997. Automatic conversion of magnetic data to depth, dip, and susceptibility contrast using the SPI method, *Geophysics,* **62,** 807–813.

Tucholke, B.E., Houtz, Robert, E. & Barrett, Douglas, M., 1981. Continental crust beneath the Agulhas Plateau, Southwest Indian Ocean, *J geophys. Res,* **86**(B5), 3791–3806.

Tsikalas, F., Faliede, J.I., Eldhom, O & Blaich, O., 2012. The NE Atlantic Conjugate Margins, in *Regional Geology and Tectonics: Phanerozoic Passive Margins, Cratonic Basins and Global Tectonic Maps*, pp. 140–201, eds David, G. & Roberts, B.P., Exploration Operation Co. Ltd.

Urien, C.M., 2001. Present and future petroleum provinces of southern South America, Chapter 19, *AAPG. Memoir,* **74,** 373–402.

Urien, C.M. & Ewing, M., 1973. Recent sediments and environment of southern Brazil, Uruguay, Buenos Aires and Rio Negro continental shelf, in *The Geology of Continental Margins,* pp. 157–177, eds Burke, C.A. & Drake, C.L., Springer-Verlag.

Urien, C.M. & Zambrano, J., 1996. Estructura del margen continental, in *Geología y Recursos Naturales de la Plataforma Continental Argentina*, pp. 29–65, eds Ramos, V.A. & Turic, M.A., Relatorio XIII° Congreso Geológico Argentino y III° Congreso de Exploración de Hidrocarburos.

Urien, C.M. & Zambrano, J., 1970. Estructura de la terraza continental del sur de Brasil y Argentina (hasta los 49º de latitud sur), in *Simposio sobre los resultados de investigaciones del manto superior con énfasis en América Latina,* vol. 2, pp. 489–500, Buenos Aires.

van der Meijde, M., Julià, J. & Assumpção, M., 2013. Gravity derived Moho for South America, *Tectonophysics,* **609,** 456–467.

van der Meijde, M., Fadel, I., Ditmar, P. & Hamayun, M., 2015. Uncertainties in crustal thickness models for data sparse environments: a review for South America and Africa, *J. Geodyn.,* **84,** 1–18.

Verduzco, B., Fairhead, J.D., Green, C.M. & MacKenzie, C., 2004. New insights to magnetic derivatives for structural mapping, *Leading Edge,* **23,** 116–119.

Watts, A.B. & Fairhead, J.D., 1999. A process-oriented approach to modeling the gravity signature of continental margins, *Leading Edge,* **18,** 258–263.

White, R.S. & Mckenzie, D.P., 1989. Magmatism at rift zones: the generation of volcanic continental margins and flood basalts, *J. geophys. Res.,* **94,** 7685–7730.

White, R., Mckenzie, D. & O'nions, R.K., 1992. Oceanic crustal thickness from seismic measurements and rare Earth element inversions, *J. geophys. Res.,* **97**(B13), 19 683–19 715.

White, R.S., Spence, G.D., Fowler, S.R., McKenzie, D.P., Westbrook, G.K. & Bowen, A.N., 1987. Magmatism at rifted continental margins, *Nature,* **330,** 439–444.

Wijns, C., Perez, C. & Kowalczyk, P., 2005. Theta map: edge detection in magnetic data, *Geophysics,* **70,** L39–L43.

Worzel, L.J. & Shurbet, L., 1955. Gravity anomalies at continental margins, *Proc. Natl. Acad. Sci. USA,* **41,** 458–469.

Zambrano, J., 1980. Comarca de la cuenca cretácica de Colorado, in *Segundo Simposio de Geología Regional Argentina II,* pp. 1033–1070, ed. Turner, J.C.M., Academia Nacional de Ciencias.

SUPPORTING INFORMATION

Additional Supporting Information may be found in the online version of this paper:

Appendix A
Appendix B
(http://gji.oxfordjournals.org/lookup/suppl/doi:10.1093/gji/ggv433/-/DC1).

Please note: Oxford University Press is not responsible for the content or functionality of any supporting materials supplied by the authors. Any queries (other than missing material) should be directed to the corresponding author for the paper.